Systems/Circuits

A Computational Model of Direction Selectivity in Macaque V1 Cortex Based on Dynamic Differences between On and Off Pathways

Logan Chariker,[1] Robert Shapley,[2,3] Michael Hawken,[2] and Lai-Sang Young[1,3,4]
[1]School of Natural Sciences, Institute for Advanced Study, Princeton, New Jersey 08540, [2]Center for Neural Science, New York University, New York, New York 10003, [3]Courant Institute of Mathematical Sciences, New York University, New York, New York 10012, and [4]School of Mathematics, Institute for Advanced Study, Princeton, New Jersey 08540

This paper is about neural mechanisms of direction selectivity (DS) in macaque primary visual cortex, V1. We present data (on male macaque) showing strong DS in a majority of simple cells in V1 layer 4Cα, the cortical layer that receives direct afferent input from the magnocellular division of the lateral geniculate nucleus (LGN). Magnocellular LGN cells are not direction-selective. To understand the mechanisms of DS, we built a large-scale, recurrent model of spiking neurons called DSV1. Like its predecessors, DSV1 reproduces many visual response properties of V1 cells including orientation selectivity. Two important new features of DSV1 are (1) DS is initiated by small, consistent dynamic differences in the visual responses of OFF and ON Magnocellular LGN cells, and (2) DS in the responses of most model simple cells is increased over those of their feedforward inputs; this increase is achieved through dynamic interaction of feedforward and intracortical synaptic currents without the use of intracortical direction-specific connections. The DSV1 model emulates experimental data in the following ways: (1) most 4Cα Simple cells were highly direction-selective but 4Cα Complex cells were not; (2) the preferred directions of the model's direction-selective Simple cells were invariant with spatial and temporal frequency (TF); (3) the distribution of the preferred/opposite ratio across the model's population of cells was very close to that found in experiments. The strong quantitative agreement between DS in data and in model simulations suggests that the neural mechanisms of DS in DSV1 may be similar to those in the real visual cortex.

Key words: computational model; direction selectivity; mechanisms; motion perception; ON/OFF pathways; primary visual cortex

Significance Statement

Motion perception is a vital part of our visual experience of the world. In monkeys, whose vision resembles that of humans, the neural computation of the direction of a moving target starts in the primary visual cortex, V1, in layer 4Cα that receives input from the eye through the lateral geniculate nucleus (LGN). How direction selectivity (DS) is generated in layer 4Cα is an outstanding unsolved problem in theoretical neuroscience. In this paper, we offer a solution based on plausible biological mechanisms. We present a new large-scale circuit model in which DS originates from slightly different LGN ON/OFF response time-courses and is enhanced in cortex without the need for direction-specific intracortical connections. The model's DS is in quantitative agreement with experiments.

Received Oct. 27, 2021; revised Jan. 25, 2022; accepted Feb. 21, 2022.

Author contributions: R.S. and L.-S.Y. designed research; L.C., R.S., M.H., and L.-S.Y. performed research; L.C. contributed unpublished reagents/analytic tools; L.C., R.S., and L.-S.Y. analyzed data; L.C., R.S., M.H., and L.-S.Y. edited the paper; R.S. and L.-S.Y. wrote the first draft of the paper; L.C., R.S., M.H., and L.-S.Y. wrote the paper.

This work was supported by National Institutes of Health (NIH) Grants R01 EY001472 (to R.S.) and R01 EY008300 and NIH R01 EY 15549 (to M.H.), National Science Foundation Grant 1734854 (to R.S. and L.-S.Y.), Simons Foundation Grants 691552 (to L.C.) and 891851 (to L.-S.Y.), the NIH Core Grant P30 EY13079, and the NIH Training Grant T32 EY7136. We thank the graduate students and postdoctoral fellows who participated in the experiments, Dario Ringach, Michael Sceniak, Elizabeth Johnson, Siddhartha Joshi, J. A. Henrie, Patrick Williams, Dajun Xing, Christopher Henry, and Anita Disney and Madhura Joglekar for early numerical explorations.

The authors declare no competing financial interests.

Correspondence should be addressed to Lai-Sang Young at lsy@cims.nyu.edu.

https://doi.org/10.1523/JNEUROSCI.2145-21.2022

Introduction

This paper is about direction selectivity (DS) in the primary visual cortex, V1, of macaque monkeys. Many neurons in layer 4Cα in V1 have DS (Hawken and Parker, 1984; Hawken et al., 1988; Saul et al., 2005; also, see Results). However, the Magnocellular cells (M-cells) of the lateral geniculate nucleus (LGN) that provide feedforward input to layer 4Cα are not direction-selective (Wiesel and Hubel, 1966; Kaplan and Shapley, 1982; Hicks et al., 1983; Derrington and Lennie, 1984), implying that DS is an emergent property in V1. What has been lacking up to now is a theoretical understanding of the mechanisms of cortical DS. In this paper, we present a biologically realistic model of macaque

V1 that we call DSV1. DS in the DSV1 model is in good agreement with V1 data, and so we can use the model to gain insight into the mechanisms of cortical DS.

DS can result when the time courses of signals vary with location in a neuron's visual receptive field (Reichardt, 1961), a property known as spatiotemporal inseparability (STI; Adelson and Bergen, 1985; Watson and Ahumada, 1985). Up until recently, most proposed theories of the biological origin of STI have relied on mechanisms that were either not biological or not plausible for macaque V1 (for more detail, see Discussion). To explain STI, the DSV1 model makes use of the ON/OFF hypothesis (Chariker et al., 2021) which is that ON and OFF M-cells have small differences in response time course and consequently the feedforward input to 4Cα cells possesses DS. Central to the ON/OFF hypothesis is that DS is found most often in Simple cells in Layer 4Cα (Results), cells that are known to receive direct LGN input (Reid and Alonso, 1995; Chatterjee and Callaway, 2003). Further, STI occurs naturally because ON and OFF LGN cells project to distinct subregions of Simple cell receptive fields (Hubel and Wiesel, 1962; Reid and Alonso, 1995).

There is more to DS in V1 than STI in its feedforward input. A comprehensive model of the V1 cell population is needed to understand cortex's response, and to identify intracortical mechanisms that may enhance or degrade the feedforward DS. We built DSV1 to model DS in the responses of a large population of cells in V1 cortex. DSV1 is a recurrent, excitatory-inhibitory network of spiking neurons. Like its predecessors (Chariker et al., 2016, 2020), DSV1 has many of the same basic visual response properties as the macaque V1 population, accurately simulating distributions of firing rates, of orientation selectivity, of spatial frequency (SF) selectivity, and the existence of Simple and Complex cell subpopulations. The DSV1 model adds the ON/OFF hypothesis (Chariker et al., 2021) and so neurons in DSV1 receive feedforward input that has DS. Given the influential view of Douglas and Martin (2004) that LGN feedforward current is a small fraction of intracortical membrane currents in V1, an important issue is whether or not the feedforward input would be sufficient to initiate enough DS to match cortical data. Implementing a fully-mechanistic population model such as DSV1 allows us to answer these questions and to weigh the feedforward and intracortical contributions to DS.

The test of a model of cortical DS is how well it simulates what the cortex does. In Results, we present new experimental data on the high level of DS in the layer 4Cα Simple cell population, on the distribution of DS across the population, and approximate invariance of DS with stimulus temporal frequency (TF) and SF. Then we show that the DSV1 model's population of cells replicates all these properties of the V1 data, quantitatively. The last part of the Results is an analysis that revealed a novel, dynamic, intracortical mechanism that causes enhancement of DS in the model. The great similarity between DS in V1 and in the DSV1 model suggests that this mechanism, using the known circuitry, may be operative in the cortex.

Materials and Methods

Experimental methods

Animal preparation

Adult male old-world monkeys (*Macaca fascicularis*) were used in acute experiments in compliance with National Institutes of Health and New York University Animal Use Committee regulations. The animal preparation and recording were performed as described in detail previously (Ringach et al., 2002; Henry et al., 2013). Anesthesia was initially induced using ketamine (5–20 mg/kg, i.m.) and was maintained with isofluorane (1–3%) during venous cannulation and intubation. For the remainder of the surgery and recording, anesthesia was maintained with sufentanil citrate (6–18 μg/kg/h, i.v.). After surgery was completed, muscle paralysis was induced and maintained with vecuronium bromide (Norcuron, 0.1 mg/kg/h, i.v.) and anesthetic state was assessed by continuously monitoring the animals' heart rate, EKG, blood pressure, expired CO_2, and EEG.

After the completion of each electrode penetration, three to five small electrolytic lesions (3 μA for 3 s) were made at separate locations along the electrode track. At the end of the experiments, the animals were deeply anesthetized with sodium pentobarbital (60 mg/kg, i.v.) and transcardially exsanguinated with heparinized lactated Ringer's solution, followed by 4 l of chilled fresh 4% paraformaldehyde in 0.1 M phosphate buffer, pH 7.4. The electrolytic lesions were located in the fixed tissue and electrode tracks were reconstructed to assign the recorded neurons to cortical layers as described previously (Hawken et al., 1988). In 49 animals, >700 V1 neurons in all cell layers were recorded in oblique penetrations. For this paper, a full data set was obtained for 94 neurons localized to layer 4Cα.

Characterization of visual properties of V1 neurons

We recorded action potentials (spikes) extracellularly from single units in V1 using glass-coated tungsten microelectrodes. Each single neuron was stimulated monocularly through the dominant eye (the nondominant eye occluded). Receptive fields were located in the visual field between 1 and 6° from the center of gaze. Stimuli were displayed at a screen resolution of 1024×768 pixels, a refresh rate of 100 Hz, and a viewing distance of 115 cm on either a Sony Trinitron GDM-F520 CRT monitor (mean luminance 90–100 cd/m^2) or an Iiyama HM204DT-A CRT monitor (mean luminance 60 cd/m^2). Monitor luminance was calibrated using a Photograph Research PR-650 spectroradiometer and linearized via a lookup table.

The response to drifting gratings was used to characterize visual response properties. In this paper, we report measurements of orientation tuning, SF and TF tuning. The response at the stimulus drift TF is called f1 and the mean firing rate is termed f0. We used the f0 response for neurons (traditionally called Complex cells) with f1/f0 ratios < 1 and the f1 response for neurons (traditionally called Simple cells) with f1/f0 ratios > 1. In the population statistics, we counted, for each TF and SF, only cells for which visually driven response exceeded four spikes/s, a condition satisfied by most of the cells recorded. All fitting was done using the Matlab function fmincon (MATLAB) where the least-squared error was used to minimize the objective function.

Orientation tuning

The responses of each neuron were recorded to different orientations between 0° and 360°, either in 20° or 15° steps. The stimuli were achromatic gratings at the preferred SF and TF, at a contrast of 64% or greater. All stimuli were presented in a circular window confined to the classical receptive field (CRF).

SF tuning

Each neuron was presented with a range of SFs, usually in ½ octave steps from 0.1 c/d to around 10 c/d. For some neurons, the upper limit was extended if the neurons had responses to higher SFs. We measured SF tuning at the preferred orientation and drift-direction as well as at the nonpreferred drift direction.

TF tuning

Each neuron was presented with a range of TFs, usually in 1 octave steps from 0.5 to 32 Hz. Measurements were made for drifting gratings at the optimal orientation in the preferred and nonpreferred directions.

DSV1 model

The main components of the DSV1 model are shown in Figure 3*A*. A visual stimulus is provided as input to the model, and we represent it by a light intensity map $L(x,t)$ where x is a location in 2D visual space and t is a time. Magnocellular ON/OFF LGN cells, modeled as leaky integrate-and-fire (LIF) neurons, receive input current equal to a spatiotemporal

filter of $L(x,t)$, and spikes generated by the LGN neurons then provide feedforward input to the neurons in layer 4Cα. The 4Cα component of the model consists of a network of E and I LIF neurons arranged in a 2D lattice spanning 1.5×1.5 mm^2 of cortex. The corresponding region of L6 of V1, known to feedback to L4 (Callaway, 1998), is also included in the model. Signal transmission from LGN to L4 is assumed to be feedforward only, whereas the interaction between L4 and L6 is bidirectional. We take the part of V1 and LGN modeled to be from ~5° eccentricity from fovea, consistent with the cells to be compared within our experimental data. More details on the individual components of the model are given below.

Visual stimuli and LGN dynamics

Visual stimuli. In this paper, the visual stimuli were drifting sinewave gratings. The light intensity map $L(x, t)$ for a drifting grating has the form:

$$L(x,t) = \{C \sin(-2\pi g \cdot x + 2\pi f t + \phi) + 1\} L_0,$$

where $x = (x_1, x_2)$ is a point in the 2D visual space, t is time (in seconds), g is SF (in c/d) in the direction of the grating, f is TF (in Hz), ϕ is the initial phase (in radians), L_0 is the mean light intensity and C is the contrast. In the model simulations in this paper, C was set to high contrast as in the experiments.

Inputs to LGN cells. The input current to an LGN cell the center of whose receptive field is located at x_0 is given by

$$I_{\pm}(t) = [I_B \pm Q(t)]^+,$$

where

$$Q(t) = Q_0 \int_0^{\infty} \int_{-\infty}^{\infty} K(s) A(x_0 - x) L(x, t - s) dx ds.$$

Here, the $\pm$ sign is for ON and OFF-cells respectively, I_B is background current, $K(s)$ and $A(x)$ are the temporal and spatial kernels of the LGN cell, Q_0 is a constant to be adjusted, and $[]^+$ denotes the maximum of the bracketed value and 0.

LGN spatial kernel. The spatial kernel is a difference of Gaussians

$$A(x) = \frac{a}{\pi \sigma_a^2} \exp\left(-\left|\frac{x}{\sigma_a}\right|\right) - \frac{b}{\pi \sigma_b^2} \exp\left(-\left|\frac{x}{\sigma_b}\right|\right),$$

with a = 1.0, b = 0.74, $\sigma_a = 0.0894$, $\sigma_b = 0.1259$ (Zhu et al., 2009); σ_a and σ_b are chosen to make the center part of the receptive field correspond to a Gaussian with SD ~0.05° (Derrington and Lennie, 1984). The preferred SF of the spatial kernel $A(x)$ is 2.5 c/d.

LGN temporal kernels. Each LGN cell is assigned a temporal kernel $K(t)$. All OFF-cell kernels are identical and have the form (adapted from Zhu et al., 2009):

$$K_{OFF}(t) = \frac{t^6}{\tau_0^7} \exp\left(-\frac{t}{\tau_0}\right) - \frac{t^6}{\tau_1^7} \exp\left(-\frac{t}{\tau_1}\right),$$

with $\tau_0 = 3.66$ ms and $\tau_1 = 7.16$ ms. Parameters are chosen following guidance from temporal kernels derived in experiments (Reid and Shapley, 2002) and the TF response of LGN cells, ensuring the peak response occurs at ~10 Hz (Derrington and Lennie, 1984). Note that K_{OFF} is positive before the zero crossing, as the polarity of the LGN cell is implemented in the sign of +/− in the expression for I(t), not in the kernel.

Differences between ON and OFF temporal kernels are introduced (following Chariker et al., 2021) to produce directional preference in the input received from LGN cells (see Results). A variety of ON cell temporal kernels is used in the model following the diversity in ON cell temporal kernels sampled experimentally (Reid and Shapley, 2002). We use the notation (a,b) to denote the temporal kernel $K_{a,b}$ defined in Results; Table 1 shows the distribution of kernels given to the ON cells.

Table 1. Distribution of kernel shapes among model ON-center LGN neurons

Kernel	(1.7, 0.8)	(1.6, 0.7)	(1.1, 0.5)	(1.0, 0.4)
Probability	10%	30%	30%	30%

Kernel shapes are given in (a,b) notation, corresponding to the kernels $K_{a,b}$ defined in Results.

A (1,1) kernel is identical to the OFF cell kernel K_{OFF}, and an (a,b) kernel is equal to K_{OFF} multiplied by a before the zero crossing and by b after the zero crossing. Each of the above kernels has a/b approximately equal to 2, which is shown by Chariker et al. (2021) to produce DS in the feedforward input to V1 at TFs below ~ 6 Hz. ON cell kernels are also given a delay of 9–11 ms, shown to produce DS in the feedforward input to V1 at TFs above ~4 Hz (see Results; Chariker et al., 2021).

For ½ of the model ON cells, the part of the temporal kernel after the zero crossing is stretched out in time to reduce the total kernel area to 0, as many experimentally sampled ON cell temporal kernels are approximately biphasic (Reid and Shapley, 2002). We found that at low TFs (4 Hz and below) adjusting the area to zero in this way significantly reduces the DS in the feedforward input to V1 cells, and consequently we left ½ of the ON cell kernels unchanged.

Dynamic equations. LGN responses are modeled with noisy-LIF (NLIF) equations with $I_{\pm}(t)$ as input (Lin et al., 2012). The membrane potential V of an LGN neuron is assumed to satisfy

$$V' = -\tau_{leak} V + I_{\pm}(t) + N(t),$$

with spiking threshold at ~1 and reset to 0. Here, τ_{leak} is a constant and $N(t)$ is a noise term.

As the firing rates of LGN cells are known to saturate under strong drive (Kaplan et al., 1987), we limit the ability of a model LGN cell to produce spikes in rapid succession by adding a brief increase to the spiking threshold immediately after a spike. This has the effect of lowering LGN firing rate when strongly driven more than when weakly driven. Implementing this mechanism causes the LGN firing rate response as a function of TF to match experimental data more closely (Levitt et al., 2001).

Cortical components

The primary focus of the DSV1 model is on the feedforward inputs from LGN → layer 4Cα (L4), the input layer to V1 in the Magnocellular stream, and the interactions of these inputs with intracortical dynamics. A third component of DSV1 is layer 6 (L6) of V1, with which L4 is known to interact (Callaway, 1998). DSV1 is descended from models by Chariker et al. (2016, 2018, 2020): mechanistic, computational models of cortical function and mechanisms. The model by Chariker et al. (2020) replicates successfully many functions of V1, such as orientation and SF selectivity, contrast response, the production of γ rhythms, and the presence of Simple and Complex cells. Its neurons do not, however, have DS. DSV1 deviates substantially from its predecessors in having different dynamics of the modeled LGN ON and OFF cells, and in how the LGN cells are connected to V1 neurons, as this is where DS in the model originates. This part of the model is discussed in detail in Results. The modeling of L4 and L6 in DSV1 is quite similar but not identical to Chariker et al. (2020). We first recall the main features of DSV1 that are largely unchanged before discussing what is different.

LGN inputs

As in its predecessors, the number of LGN inputs, nLGN, to an E-cell is randomly sampled from the distribution shown in Table 2 and for cells with four to six inputs, 2/3 are assigned templates with two ON/OFF stripes and the remaining with three stripes.

Dynamics of 4Cα neurons

Layer 4Cα consists of a network of excitatory (E) and inhibitory (I) neurons with membrane potentials evolving according to a set of LIF equations. Potentials are denoted by V_i^E and V_i^I for E- and I-neurons, respectively, with i = neuron index. Neurons spike when V reaches a

Table 2. Distribution of nLGN to model 4Cα E-neurons

nLGN	1	2	3	4	5	6
Prob.	10.5%	20%	2%	21%	32.5%	14%

Each 4Cα excitatory (E) neuron is given nLGN feedforward inputs with the probabilities given in the table.

threshold potential of $V_{thresh} \sim 1$. Upon reaching the threshold, V is instantaneously reset to a resting potential value of $V_{rest} = 0$, remaining for an absolute refractory period of $t^E_{ref} = 2$ ms for E and $t^I_{ref} = 1$ ms for I. While not in the refractory period, V obeys the LIF equation (Knight, 1972):

$$\frac{dV_i^Q}{dt} = -\frac{1}{\tau^Q_{leak}} V_i^Q - g_i^{QE}(V_i^Q - V^E) - g_i^{QI}(V_i^Q - V^I), \quad \text{(M1)}$$

where Q = E or I denotes the neuron type; $V^E = 14/3$ and $V^I = -2/3$ are the excitatory and inhibitory reversal potentials; and g^{QE} and g^{QI} are the excitatory and inhibitory conductances. g^{QE} is a sum over all excitatory postsynaptic conductances (EPSC) generated by the presynaptic excitatory spikes of layer 4Cα, layer 6, and LGN, as well as from independent, Poisson-timed kicks modeling the effects of ambient neurotransmitter. g^{QI} is a sum of inhibitory postsynaptic conductances (IPSC) from the presynaptic inhibitory spikes in layer 4Cα. In the case of Q = E, an additional slow time course IPSC is generated from each presynaptic inhibitory spike. Details on the EPSC and IPSC time courses can be found in Chariker et al. (2018).

Layer 4Cα (L4)

We modeled nine hypercolumns (HCs) of 4Cα. Each HC measures 0.5 mm × 0.5 mm and is divided into regions within which cells are intended to have similar orientation preferences. Following Beaulieu et al. (1992), we used cell densities of ~4000 neurons per HC, 3/4 of which are E-cells and the rest are I-cells. The I-neurons are assumed to be a homogeneous population of local-circuit basket cells, a reasonable approximation for layer 4Cα (DeFelipe et al., 1999). E-neurons and I-neurons are uniformly distributed in the model cortex, and their dynamics are governed by conductance based integrate-and-fire equations. The probability of connection between model cells is dependent on distance in the cortex and on cell types (E or I), while the strength of connection is independent of distance (based on Oswald and Reyes, 2011). For presynaptic E-neurons, the distance dependence of the connection probabilities are given by Gaussians with standard deviation SD $= 200/\sqrt{2}$ μm; for presynaptic I-cells, SD $= 125/\sqrt{2}$ μm (Fitzpatrick et al., 1985; Yoshioka et al., 1994). Peak connection probability between E-cells is ~15% on average. I-cell connections are denser. Following Holmgren et al. (2003) and Oswald and Reyes (2011), we set peak I-to-I connection probability at cortical distance = 0 to be 60%.

The numbers of connections and cell densities imply that on average, an E-cell has ~200 presynaptic E-cells and ~100 presynaptic I-cells; for an I-cell, the corresponding numbers are ~750 E-cells and ~100 I-cells. In addition to cortical inputs, layer 4Cα E-cells and I-cells receive monosynaptic input from one to six Magnocellular LGN neurons (more details given in Results).

Feedback from layer 6 (L6)

In DSV1 as in the real cortex, L4 and L6 interact continuously in a self-adjusted feedback loop. The details of the L4-L6 feedback loop were specified by Chariker et al. (2020). The goal of Chariker et al. (2020) was to construct a model that could simulate the response of V1 over a wide range of stimulus contrast, simulating approximate contrast invariance, and the L4-L6 feedback loop played a large role in model performance. In this paper, the model was used to simulate only experiments that employed high contrast stimuli and thus the L4-L6 feedback loop was working only at one contrast level throughout. We refer the reader to Chariker et al. (2020) for a complete documentation of the model details given in the SI of that paper.

Two new features of DSV1

(1) Firing rate homeostasis

Without intervention, firing rates of Simple E-cells in DSV1 varied widely, more so than in its predecessors in part because of the use of variable amplitudes in the temporal kernels of its LGN cells. Homeostatic mechanisms that could support adjustment of synaptic input to stabilize firing rates are known to be present in cortex (Turrigiano, 2012). Homeostasis was introduced into DSV1 by giving Simple E-cells in L4 that are very high firing more I-input (e.g., 5–10 more I-cell inputs in addition to the usual complement of ~100 I cell inputs). This produced a small reduction of firing rates in the Simple cells with the highest firing rates. It also had the effect of reducing an unwanted correlation in DSV1 between high firing rate and low DS, a correlation that was not present in the cortical data.

(2) Adaptation at low TFs

DSV1 is the first in this line of models to consider a full range of TF. To control the build-up of excessive spiking of Complex cells at low TF, it is necessary to incorporate a form of spike rate adaptation. Adaptation mechanisms are also known to be present in the real cortex (Barkai, 2005; Adelman et al., 2012). Adaptation made it harder for an E-neuron to continue to fire after a burst of 7 consecutive spikes are fired within 150 ms. While adaptation is activated, every I-spike received by the E-cell comes with an additional slow time course

$$G^{adapt}(t) = S^{EI}\left(\frac{1}{\tau^{decay}}\exp\left(-\frac{t}{\tau^{decay}}\right) - \frac{1}{\tau^{rise}}\exp\left(-\frac{t}{\tau^{rise}}\right)\right),$$

with time constants $\tau^{\text{rise}} = 5$ ms and $\tau^{\text{decay}} = 100$ ms, and with synaptic strength S^{EI} equal to the usual I-to-E strength. This time course resembles that of $GABA_B$, known to be present in V1 (Zilles et al., 2004).

Model parameters

The synaptic coupling strengths are an important part of the model. They are set in the same way as in previous models (Chariker et al., 2016, 2020) with the use of spike firing data and intracellular recording data as guides. The coupling strength between E-cells in L4, termed S^{EE}, was set to 0.023, consistent with experimental data (Stratford et al., 1996). The coupling strength from I- to E-cells, S^{EI}, was calculated to be $2.16 \cdot S^{EE}$ based on firing rates and intracellular data (cf. Chariker et al., 2016, their Materials and Methods). The coupling strength between I-cells, S^{II}, was set to be $0.65 \cdot S^{EI}$. The remaining coupling strength S^{IE}, the coupling strength from E to I, was determined to be $\sim 0.26 \cdot S^{EE}$ by simulating a range of values of S^{IE} and finding what value of S^{IE} was compatible with the mean background firing rate of E-cells as measured experimentally. Based on the literature, we set the LGN synaptic coupling weights to be $S^{E,LGN} = 2.3 \cdot S^{EE}$ and $S^{I,LGN} = 2.85 \cdot S^{EE}$. The coupling coefficients for L6, based on previously published work (Stratford et al., 1996) were $S^{E,L6} = 0.36 \cdot S^{EE}$ and $S^{I,L6} = 0.087 \cdot S^{EE}$. Table 3 gives values for model parameters.

Statistical comparison of the cumulative distribution functions (CDFs) of model and data

We used a bootstrap procedure to calculate the similarity or dissimilarity between the CDF that describes the Pref/Opp ratio of experimental data and the CDF of the cells in the DSV1 model (Results; Fig. 7). We generated 1000 sample distributions of DS (= Pref/Opp) from the model, each having the same number of cells as the data distribution: $N = 62$ in the case of Simple cells and $N = 32$ in the case of complex cells. We used sampling with replacement. Then we calculated the CDF for each sample and the data by binning the sample distributions and the data distribution in the same way. The CDF had seven bins: 1–1.414, 1.414–2, 2–2.828, 2.828–4, 4–5.66, 5.66–8, and >8. That was done so that each bin of the CDF had O(10) cells. Then we calculated the summed squared deviation (SSD) between each sample CDF and the CDF of the full population of model cells: 2031 Simple cells for the Simple cell CDF and 914 Complex cells for the Complex cell CDF and also the SSDs for the data CDFs for both Simple and Complex cells. The statistical comparison was

Table 3. Model parameter values

Parameter	Value	Description
τ_{leak}	0.1 ms^{-1}	LGN cell membrane leak rate [see V(t) equation in Materials and Methods]
I_B	0.1 ms^{-1}	LGN background current [see I(t) equation in Materials and Methods]
C	0.109	Input current prefactor [see Q(t) equation in Materials and Methods]
S^{EE}	0.0230	E⟶E synaptic strength
S^{EI}	0.0497	I⟶E synaptic strength
S^{IE}	0.0059	E⟶I synaptic strength
S^{II}	0.0321	I⟶I synaptic strength
S^{ELGN}	0.0529	LGN⟶E synaptic strength
S^{ILGN}	0.0655	LGN⟶I synaptic strength
S^{EL6}	0.0080	L6⟶E synaptic strength
S^{IL6}	0.0020	L6⟶I synaptic strength

LGN model parameters and synaptic coupling strengths between LGN, 4Cα E and I, and L6 are shown.

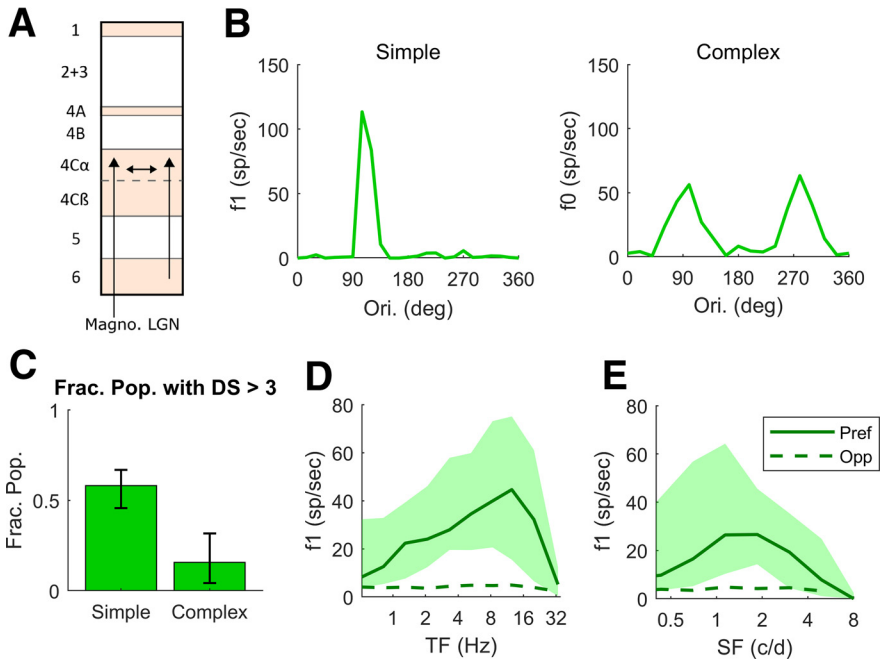

Figure 1. Experimental Data on DS and firing rates as a function of TF and SF in macaque layer 4Cα. ***A***, Diagram showing a cross section of the layers of V1, with arrows indicating the recurrent interaction within layer 4Cα, feedforward inputs to layer 4Cα from LGN and feedback to layer 4Cα from layer 6. All data in this figure are from cells recorded in layer 4Cα. ***B***, Orientation tuning curves for a highly DS Simple cell and a non-DS Complex cell. ***C***, Fraction of Simple and Complex cells with DS (= Pref/Opp) > 3. In our sample, 36 of 62 Simple cells and 5 of 32 Complex cells had DS > 3, with 95% confidence intervals. ***D***, TF tuning curves of Pref and Opp firing rates in Simple Cells with DS > 3. The thick solid curve shows median Pref firing rate and dashed curve shows median Opp firing rate. Quartiles indicted by the shading around the median. ***E***, SF tuning curves; same setup as in ***D***. Note that the median rate here is lower because there is a range of preferred SF across the population therefore the median underestimates the median of the rate at the preferred SF.

between the SSDs for the data (Simple and Complex) CDFs and the distribution of SSDs for the 1000 samples for the Simples and 1000 samples for the Complexes. The result was that the SSD for the Simple cell data CDF was 0.91 * SD for the 1000 samples, and the SSD for the Complex cell data CDF was 0.21 * SD for the 1000 samples. This leads to $p > 0.2$ for Simple cells and $p > 0.7$ for Complex cells.

Results

Here is a brief guide to the Results section: it contains (1) data that establish that there is a high proportion of Simple cells in macaque layer 4Cα that are direction-selective, and the broad-band nature of their DS; (2) the ON/OFF hypothesis by Chariker et al. (2021) about DS in the feedforward input to V1; (3) the design of the DSV1 model; (4) a comparison of DS in data and model, and (5) an analysis of the DSV1 model that shows how cortex boosts the DS present in its feedforward inputs.

Experimental data on DS in macaque V1, layer 4Cα

Action potentials (spikes) were recorded extracellularly from single units in macaque V1 using tungsten microelectrodes. We measure responses to drifting, achromatic, sinusoidal gratings to characterize visual response properties (see Materials and Methods). Stimulus contrast in these experiments was 64% or greater. In 49 animals, the activity of hundreds of V1 cells in all cell layers was recorded in oblique penetrations; complete data were obtained for ~700 cells that could be assigned accurately to a cell layer. The data in this paper are from neurons localized to layer 4Cα on the basis of histology (Fig. 1*A*; see Materials and Methods). Cortical cells were classified as Simple and Complex cells conventionally, on the basis of the modulation ratios (f1/f0) of their responses to drifting gratings (Skottun et al., 1991; Ringach et al., 2002; Materials and Methods). We present in Figure 1*C–E* data for 94 cells in layer 4Cα: 62 Simple cells and 32 Complex cells.

A large fraction of the cells recorded in layer 4Cα had a high value of DS. Representative examples of single-cell responses are shown in Figure 1*B*. The response versus orientation of one 4Cα Simple cell is shown in the left panel and of one Complex cell in the right panel. The data in the graphs of Figure 1*B* are the responses to drifting gratings at the (SF, TF) combination that produces the highest response at the stimulus drift TF (f1) in the Simple cell or the highest mean firing rate (f0) in the Complex cell. The measure of DS that we use throughout the paper for both experimental data and model responses is the ratio Pref/Opp. For Simple cells, Pref is taken to be the f1 response in the orientation of maximal response (for Complex cells we use f0), and Opp for Simple cells is the f1 response at 180° from the Pref direction (for Complex cells again we use f0). Across the population of 4Cα Simple cells in our sample, the fraction with DS > 3 is 0.58 (Fig. 1*C*); the fraction of 4Cα Complex cells with DS > 3 is only 0.16 (Fig. 1*C*; cf. Hawken et al., 1988). The DSV1 model emulates the much higher incidence of DS in Simple cells, as shown later in Results.

An important property of DS in layer 4Cα is the broad-band character of DS (Fig. 1*D*,*E*) in Simple cell responses. In the experiments, we measured responses at preferred and opposite-to-preferred directions over a wide range of TF and SF for 53 Simple and 29 Complex cells. The preferred and opposite-to-preferred directions identified at the peak of the ori-tuning curve as in Figure 1*B* were the same directions for all TF and SF, i.e., the preferred direction remained consistent over the entire range of

response. In Figure 1*D*, the median Pref (f1) response (solid curve) across the population of 4Cα Simple cells that had high DS (Pref/Opp > 3; 26 cells) is much larger than that of Opp (dashed curve) across the full range of TF to which the cells respond, not just at or around the peak response near 10 Hz. We also measured DS as a function of SF in the high DS Simple cell population (Fig. 1*E*; 25 cells). As with TF, Pref responses are larger than Opp over the full range of SF that is effective in driving V1. The broadband character of DS in 4Cα neurons is reproduced in the DSV1 model, as shown later in Results.

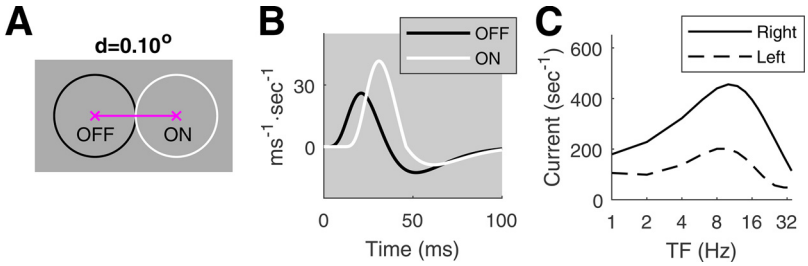

Figure 2. Summed response from a pair of ON and OFF LGN cells (redrawn from Chariker et al., 2021). ***A***, ON-OFF pair separated by d^o, with ON to the right of OFF; the circles represent 1 SD of the center Gaussian of each LGN receptive field. ***B***, Relative to the OFF-kernel (black), the ON-kernel (white) has a 10-ms delay and is of type (1.6, 0.7; see Results, DSV1 model description). ***C***, Right versus left responses (summed ON and OFF currents) as functions of TF, at SF = 2.5 c/d.

Theory of DS in feedforward inputs and OFF-ON dynamics

First we describe the theory proposed by Chariker et al. (2021) that is embedded in the DSV1 model, and then in the following section we describe the model itself. The basic concept developed by Chariker et al. (2021) is that different response time-courses of OFF and ON LGN neurons afferent to a cortical cell would result in DS in their summed responses that comprise the feedforward input to 4Cα neurons.

Reducing two rows of OFF and ON LGN cells to an OFF-ON pair the receptive fields of which are separated by d degrees (Fig. 2*A*) and assuming the responses of individual LGN cells are functions of sinusoidal form (a simplification), we analyzed by Chariker et al. (2021) the summed response of the OFF-ON pair to left and right-moving gratings. The key findings can be summarized as follows:

1. DS is equivalent to asymmetric ON/OFF phase differences in response to left and right gratings: the grating that elicits the smaller phase difference (i.e., where ON and OFF elicit firing more in-phase) is the preferred direction. This idea, known from earlier work (Watson and Ahumada, 1983, 1985), is behind much of the theory.
2. Two mechanisms for inducing such asymmetric ON/OFF phase differences are: (1) delay in the ON-response and (2) different time kernels of ON versus OFF cells, with the ON-kernel having a taller positive lobe. Mechanism (1) is effective at high TF; mechanism (2) at low TF (Fig. 2*B*). These two mechanisms combined produce a consistently preferred direction, from OFF to ON, with roughly the same amount of DS over a broad range of TF, as illustrated in Figure 2*C*.
3. If the ON/OFF separation d is smaller than half the period of the stimulus grating, then directional preference of the OFF-ON pair will be consistent over the entire range of SF visible to the LGN pair (Chariker et al., 2021). This means, for example, that values of d should be $< 0.10°$ of visual angle for an eccentricity of ~5°. In general, optimal SF, receptive field size, and d scale with eccentricity.

The findings above describe how DS in summed ON-OFF LGN response is produced in an idealized setting. It is understood that there will be much more variability in the real brain.

DSV1 model description

The general physical layout of the DSV1 model is shown in Figure 3*A*. The model has three components: Magnocellular LGN cells, layer 4Cα (L4) and layer 6 (L6) of the primary visual cortex (V1; compare Fig. 1*A*). The region of cortex modeled represents an area of roughly $0.75° \times 0.75°$ on the retina located at ~5° eccentricity. Our primary focus is L4, populated by 36,000 Excitatory (E) and Inhibitory (I) neurons, coupled with synapses that have realistic conductances. All the neurons in the model obey the LIF differential equation (Knight, 1972) written in Materials and Methods. The DSV1 model, like its predecessors (Chariker et al., 2016, 2020) is highly recurrent, consistent with the modern view of visual cortical function (Douglas and Martin, 2004). The model cortex gets all its LGN input from one eye only; the inclusion of ocular dominance columns would not impact the character of the feedforward input from LGN to cortical cells.

Inputs to DSV1 are visual stimuli represented as time-dependent light-intensity maps $L(x,t)$ where x denotes the location on the retina (or on the LGN sheet) and t denotes time. Once $L(x,t)$ is presented to the model, LGN computes a response, which is passed to L4, and dynamic interactions within L4 and between L4 and L6 produce a response. Only drifting gratings are used as stimuli in the current study because most experimental data about DS were obtained with such stimuli, but the DSV1 model's capabilities are not limited to this class of visual stimuli.

DSV1 deviates from its predecessors (Chariker et al., 2016, 2020) in its OFF-ON LGN dynamics and in the design of LGN "templates," referring to configurations of LGN cells projecting to a cortical neuron. These modifications, which follow prescriptions by Chariker et al. (2021), are necessary to simulate cortical DS; in our earlier models that had ON and OFF LGN cells with the same response dynamics (Chariker et al., 2016, 2020), model neurons were not direction-selective. The architecture of the network, the equations governing the dynamics, and the parameters used are similar though not identical to those by Chariker et al. (2020); they are described in detail in Materials and Methods. Below, we focus on DSV1's most significant deviations from its predecessors, namely, LGN dynamics and thalamo-cortical convergence.

LGN dynamics

In DSV1, ON and OFF cells have different dynamics, i.e., visual response time courses, following the prescription by Chariker et al. (2021).

First, we introduce a delay in the response of ON LGN cells with respect to OFF. Such a delay is consistent with retinal circuitry required for the sign inversion in the ON pathway (Masland, 2012) and with direct measurements of LGN visual responses (Reid and Shapley, 2002; Jin et al., 2011). In DSV1 the time delay between ON and OFF varied between 9 and 11 ms (Fig. 2*B*).

Following Reid and Shapley (2002), we model the temporal kernel shapes of OFF and ON cells as follows: let the OFF-kernel

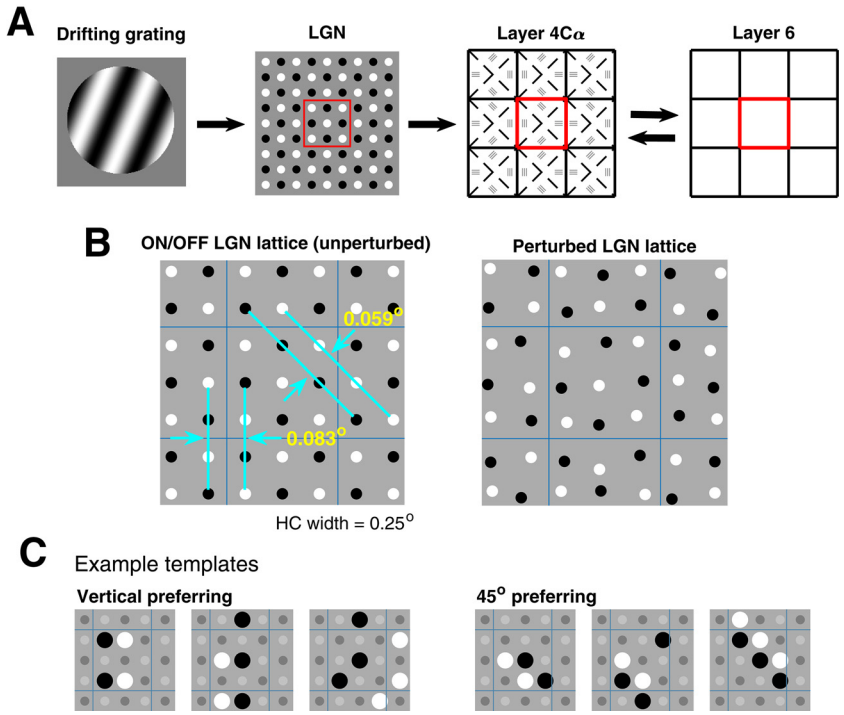

Figure 3. The DSV1 model and its LGN templates. ***A***, General layout of the three components of the DSV1 model. The visual stimulus is represented by the drifting grating on the left. This information goes to the sheet of Magnocellular LGN cells. Each cell computes a response R(t) as described in Results. LGN outputs are then passed to layer 4Cα of V1, the primary input layer of the Magno stream. Layer 4Cα receives feedback from layer 6. ***B***, LGN sheet showing ON-OFF separation distances: ON cells in white, OFF cells in black; square lattice unperturbed (left), perturbed (right). ***C***, Six example LGN templates, three for vertical and three for 45°, with nLGN = 4, 5, 6.

$K_{OFF}(t) = K(t)$ be as defined in Materials and Methods. Using $K^+(t) = \max\{0, K(t)\}$ and $K^-(t) = \min\{0, K(t)\}$ to denote the positive and negative parts of $K(t)$, we consider the family of temporal kernels $K_{a,b}(t)$ defined by:

$$K_{a,b}(t) = aK^+(t) + bK^-(t).$$

In this notation, $K_{OFF}(t)$ has the structure (1,1). It is shown by Chariker et al. (2021) that a kernel $K_{a,b}(t)$ with $a > b$ produces a phase lag relative to $K_{1,1}(t)$. In the DSV1 model, ON-cells had temporal kernels with a variety of structures (a, b) with $a/b \sim 2$ (consistent with previously published data; Reid and Shapley, 2002); they range from (1.7, 0.8) to (1.0, 0.4) drawn randomly for each cell. The OFF kernel and a typical ON kernel are illustrated in Figure 2*B*.

Template design

One of the features that distinguishes the DSV1 model and its predecessors (Chariker et al., 2016, 2018, 2020) from other existing models of the visual cortex is their realistic depiction of the small number of LGN cells per unit area of the visual field in the M-cell–layer 4Cα pathway. Two independent estimates based on M-retinal ganglion cell density (Silveira and Perry, 1991) and on macaque LGN data (Connolly and Van Essen, 1984) point to an average of approximately nine LGN cells projecting to an area of 0.25° × 0.25° in the visual field, roughly the retinal projection to one V1 HC at 5° eccentricity. Using different inferences, Garcia-Marin et al. (2019) suggested a somewhat higher figure for LGN-V1 convergence. Whichever estimate one uses, the M-cell LGN input to V1 cortex is very sparse. Given that the rows of ON and OFF LGN cells cannot be too far apart to ensure a consistent directional preference as seen in data [Chariker et al., 2021, their see Figure 1 and Result (3) in the summary of results], the LGN sparseness poses a significant challenge to modeling.

In DSV1, we model the locations of LGN cells by a perturbed square lattice of alternating ON/OFF cells as shown in Figure 3*B*. We start from a regular lattice with 9 LGN cells/HC (Fig. 3*B*, left), and perturb each cell's position in the lattice with independent Gaussians with SD = 0.01° resulting in the somewhat irregular mosaic on the right. In the (unperturbed) lattice, there are very few discrete choices of ON-OFF distances. Between two vertical rows, the distances are multiples of 0.083°, and between two diagonal lines making 45° with the vertical, the distances are multiples of 0.059°. Both are within a favorable range of d (Chariker et al., 2021).

By an LGN "template," we refer to a configuration of LGN cells that forms the inputs to a cortical cell; translations of the same configuration are regarded as coming from the same template. In the DSV1 model, there are four distinct collections of LGN templates; they prefer 0° (which we define to be vertical), 45°, 90°, and 135°. The latter two collections are obtainable from the first two by a 90° rotation, so we need only to be concerned with vertical and 45° templates. The number of LGN afferents to a cortical cell in the model is between 1 and 6, with slightly less than half of the cortical cells receiving five or six LGN inputs. Those numbers are based on the sparseness of LGN together with results by Angelucci and Sainsbury (2006) on thalamo-cortical convergence. The chosen LGN templates consist mostly of configurations where the ON-OFF rows are as close to each other as possible. Several examples of the templates used are shown in Figure 3*C*. We switched from the perturbed hexagonal lattice used previously (Chariker et al., 2016, 2018) because the design of templates with ON/OFF separations $<0.1°$ is simpler using a square lattice but we duplicated all of the results in this paper using hexagonal lattices (data not shown), proving that the results are not tied to the specific lattice choice.

Connection of LGN cells to V1 cells

Following are the rules for assigning to each V1 cell a group of LGN cells that project to it. In layer 4Cα, we divide each HC of L4 into four wedges (Fig. 3*A*). Cells in each wedge are given the intended orientation indicated by the three bars drawn in that wedge, and cells near the boundary of two wedges have probability ½ of picking each of the two intended orientations. There are two main parts to LGN assignment. (1) Selection of template: from the collection of templates for that orientation, we picked randomly according to the prescribed probabilities on (a) the number of LGN cells in the template, and (b) two versus three ON/OFF subregions as described in Materials and Methods. (2)

Admissible locations: all possible translations of the configuration chosen in (1) that lie within a radius of 0.3° of the V1 cell's retinal projection are admissible and are chosen with equal probability.

To be clear, we have not built into DSV1 any capability for generating directional preference beyond DS in feedforward LGN inputs: for a cortical cell, presynaptic E-cells and I-cells are isotropically distributed, there are no special connections between cells with the same directional preference, and no long-range intracortical lateral connections in layer 4Cα. In local populations of 4Cα cells, LGN templates of opposite parity (in ON/OFF) were drawn with equal probability to avoid introducing biases in preferred directions.

Parameter choices in relation to DS (summary)

The parameters directly connected to the generation of DS and its level in the model cortex include: (1) the time delay between OFF and ON LGN cells; (2) the a/b ratio of the LGN ON time kernels; and (3) the OFF-ON separation *d*. Theoretically, the larger the quantities in (1) and (2), the more DS; our choices were constrained by data (Reid and Shapley, 2002). As for (3), d had to be $<0.1°$ to avoid reversal in directional preference (Chariker et al., 2021), it was unclear a priori if this could be feasible given the sparseness of LGN cells but we have checked that it was (see Fig. 3*B*). Other parameters followed mostly those given by Chariker et al. (2020; see Materials and Methods) and were chosen to ensure model performance with regard to visual properties such as orientation selectivity and contrast response; they do not directly impact the level of DS. Homeostasis and adaptation (Materials and Methods) also do not directly impact DS. We comment on E-I balance, a feature that will be important in the sections to follow. E-I balance plays no role in the generation of DS (which involves only LGN responses) but it controls the effectiveness of the model's feedforward LGN inputs, hence may potentially affect the level of DS in the responses of cortical cells. In DSV1 as in its predecessors, the balancing of E- and I-currents is an emergent phenomenon, one that occurs once E-firing and I-firing rates are constrained to realistic ranges.

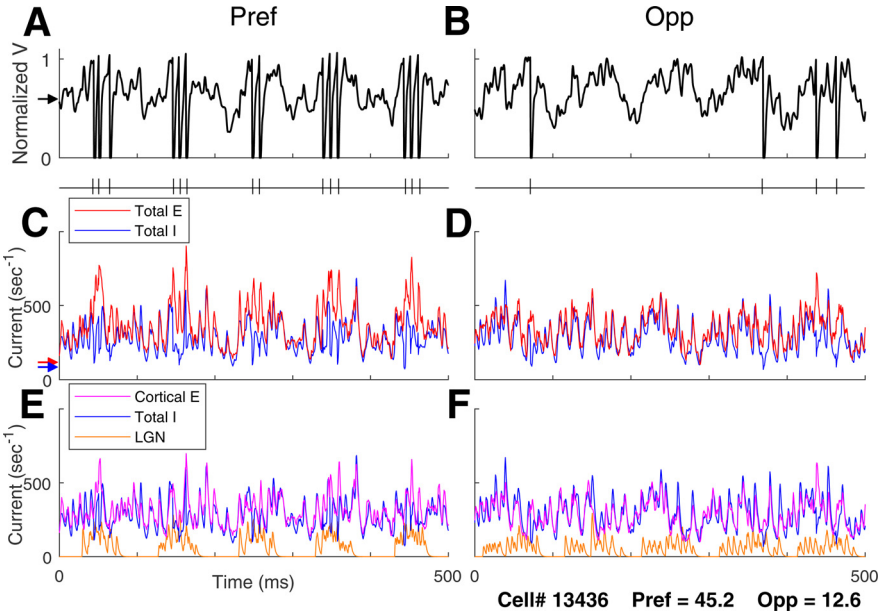

Figure 4. Voltage and input current traces in Pref and Opp directions for a model high DS Simple cell. Responses of a high DS cell in the model to drifting gratings of 3 c/d and 10 Hz, optimal for this cell. Panels ***A***, ***C***, ***E*** are for Pref; ***B***, ***D***, ***F*** are corresponding panels for Opp. ***A*** (Pref), ***B*** (Opp), Voltage traces and spike times. ***C*** (Pref), ***D*** (Opp), Total synaptic input currents: total excitatory current (= L4+L6+LGN+amb; red), negative of inhibitory current (blue). ***E*** (Pref), ***F*** (Opp), Synaptic input currents by source: LGN current (orange), cortical E-current (= L4+L6+amb; purple), negative of I-current (blue). Arrows on the left show time averages during spontaneous activity of (***A***) membrane potential (black), (***C***) total E (red) and Total I (blue) synaptic currents.

DS properties of the DSV1 model and comparison with data

Time series of membrane voltage and currents in DSV1

Comparing membrane potential and synaptic current traces in the preferred and opposite directions for DS neurons in DSV1 is revealing about the role of LGN inputs in driving cortical dynamics. Figure 4 shows voltage traces for a typical model Simple cell of high DS, in Pref (Fig. 4*A*) and Opp (Fig. 4*B*) directions when driven by an optimal stimulus grating of SF = 3 c/d and TF = 10 Hz. Spike occurrences are indicated in the plots just below the respective voltage plots. Many more spikes are fired in response to the stimulus in the preferred direction and the firing rate in the preferred direction is modulated at the stimulus TF of 10 Hz.

The plots of membrane current illustrate what is happening intracellularly in a model DS cell when it receives visual input. Figure 4*C*,*D* shows membrane synaptic currents in Pref and Opp directions. "Total E" here refers to the sum of the E-currents from L4, L6, LGN, and ambient sources (see Materials and Methods for the definition of "ambient"). Total I is the magnitude of the input I-current, plotted with a positive sign so we can compare the magnitudes of the E- and I-currents. The increase in current during stimulation can be seen by comparing to the arrows on the left; they show mean E-currents and I-currents during spontaneous activity.

Figure 4*E*,*F* shows the decomposition of Total E into LGN and "cortical-E," referring to L4+L6+amb. The cortical-E and I-currents track each other over time (Fig. 4*E*,*F*) as was documented in our previous recurrent models (Chariker et al., 2018). The covariation of these currents in γ-band oscillations is an emergent phenomenon in highly recurrent models like DSV1, producing a moment-by-moment balance that is a stronger form of E-I balance than that in classical balanced state theories (van Vreeswijk and Sompolinsky, 1996; Hansel and Sompolinsky, 1997); this behavior has been termed "tight balance" in the review by Denève and Machens (2016).

In the Pref direction (Fig. 4*C*), the E-I balance is broken roughly every 100 ms (the grating's TF = 10 Hz), when the Excitatory current is more strongly modulated by its LGN inputs. When that happens, the E-current momentarily overwhelms the I-current causing spikes to be fired. In the Opp direction (Fig. 4*D*), the LGN drive is smaller and more spread out in time. It is less effective in producing the sudden surges in excess E-current needed to drive the membrane potential over threshold. These current plots show clearly that feedforward LGN inputs in Pref and Opp directions impact cortical firing, although LGN synaptic current comprises only a small fraction of the total E-current entering a cell.

That LGN feedforward inputs should have such a large impact on Simple cell spike firing is because of the balance of excitatory and inhibitory cortical synaptic currents (van

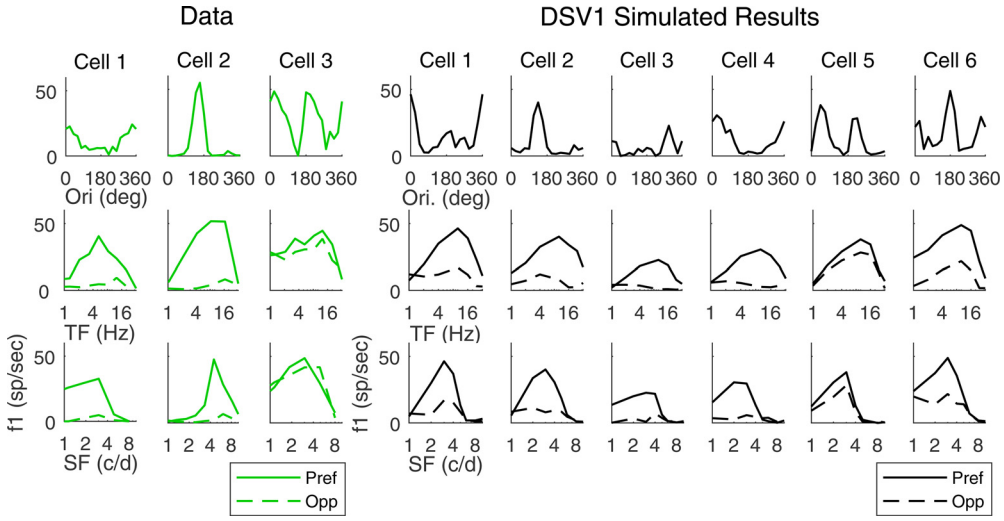

Figure 5. DS properties of single cells from experimental data and model output. Tuning curves of three recorded V1 simple cells (left) and six model simple cells (right) are shown. Top, Orientation tuning curves at optimal TF, SF. Middle, Reponses in Pref and Opp directions versus TF. Bottom, Reponses in Pref and Opp directions versus SF.

Vreeswijk and Sompolinsky, 1996; Hansel and Sompolinsky, 1997). For a cortical cell in the model, firing rate is roughly determined by the difference between its Total E-current and Total I-current; this is a direct consequence of the LIF equation (Materials and Methods). When cortical-E and I currents are approximately balanced as they are in DSV1 (Fig. 4*E*,*F*), each cortical cell's spike firing is very sensitive to the size of the modulated Feedforward input. The behavior illustrated in Figure 4 is typical for DS cells in the DSV1 model. Similar ideas about E/I balance have been used to explain the preservation of orientation tuning in layer 2/3 of mouse visual cortex (Hansel and van Vreeswijk, 2012).

Visual responses of single cells in the data and in the DSV1 model

The tuning curves of individual model cells in DSV1 indicates that their visual properties closely resemble those of typical 4Cα Simple cells in the real cortex (Fig. 5). Plotted on the left of Figure 5 are tuning curves of cells recorded in layer 4Cα (in green); on the right are the tuning curves of model Simple cells (in black). The first row shows orientation tuning, the second row shows TF responses in Pref (solid) and Opp (dashed) directions, and the third row are plots of SF responses. Cells 1 and 2 in the data have high DS. Their orientation tuning curves have only one peak over the full 360° range of orientation, and the Opp responses in the TF and SF tuning curves are much smaller than Pref responses, with no changes in directional preference across TF or SF. Cell 3 in the data is an example of a nondirection-selective Simple cell. In the group of model cells in Figure 5, cells 1–4 have high DS, cell 6 has some DS, while cell 5 has little or no DS. The DS cells in the model have much larger Pref than Opp responses across TF and SF, resembling the cells 1, 2 in the data. Also, they display a great deal of diversity in their tuning curves, as in the data.

Population data on DS

It is important to compare not only single cell examples but also population data on DS in layer 4Cα with the population data in the DSV1 model.

The first feature of the DSV1 population data is the higher incidence of DS in Simple cells than in Complex cells. For direct comparison with data, Pref and Opp for model Simple cells are measured in f1, while f0 is used for complex cells. The fraction of model Simple cells that have Pref/Opp $>$ 3 (Fig. 6*A*) is very similar to what is observed in the 4Cα data (Fig. 1*C*), and the fraction of Complex cells that have Pref/Opp $>$ 3 is much smaller, in DSV1 (Fig. 6*A*) as in the data (Fig. 1*C*). The higher incidence of DS in Simple cells than in Complex cells (Fig. 6*A*) is a direct consequence of the structure of DSV1 as explained in connection with Figure 7 below.

A second feature is the comparison of the population average TF and SF tuning in Pref and Opp directions between model and data. As in the data analysis of Figure 1, "Pref" for a Simple cell is defined as the direction that evokes the cell's maximal f1 response over all stimulus conditions (orientation, direction, SF and TF); and "Opp" refers to the response in the direction opposite to Pref. The results are that, for responses in the Pref direction, median f1 for model Simple cells (Fig. 6*B*,*C*) peaks at TF = 10 Hz and 3 c/d, and these values are similar to those found in the data (Fig. 1*D*,*E*, respectively; cf. Hawken et al., 1988, 1996). As in the data in Figure 1*D*,*E*, the Pref and Opp directions in the model neurons remain the same across TF and SF (Fig. 6*B*,*C*). Median responses in the Opp direction are much smaller than Pref responses for model Simple cells (Fig. 6*B*,*C*) across TF and SF as in the 4Cα data (Fig. 1*D*,*E*). One implication of Figure 6*B*,*C* is that DS in the DSV1 model has the same broad-band character as in the cortical data.

Population distributions of DS across the layer 4Cα population enable a direct comparison of DS in data and model (Fig. 7). Figure 7*A* shows distributions of Pref/Opp in layer 4Cα Simple cells in real cortex (green, upper panel) and in model Simple cells (black, lower panel). As in Figure 1, for each cell in the population, Pref/Opp was computed for the stimulus orientation that produced the largest Pref response. The two distributions in Figure 7*A* have very similar shapes. For instance, they have similar medians (~3.5) and similar fractions of cells with very high DS, i.e., those cells with Pref/Opp $>$ 8 (Fig. 7*A*).

The cumulative distribution functions (CDFs) of DS of Simple and Complex cells in DSV1 simulate those of the data very closely (Fig. 7*B*). Plotted on the vertical axis of Figure 7*B* is the fraction of neurons with Pref/Opp $<$ x, where x is the value of the Pref/Opp ratio on the horizontal axis. The plots indicate that a large fraction of Simple cells in layer 4Cα are directionally

selective while Complex cells usually have a small Pref/Opp ratio (Hawken et al., 1988; Fig. 6). The same is true in the DSV1 model. A bootstrapping method was used to test whether or not the CDFs of the data were significantly different from that of the model, for both Simple and Complex cell populations, by computing the summed square deviation (SSD) between model and data CDFs (see Materials and Methods for details). The probability that the Simple cell data were the same as that of the model is $p > 0.2$, while for Complex cells $p > 0.7$. The CDFs of data and model are not distinguishable statistically. Without a biologically realistic, fully mechanistic model, comparison of model DS with experimental data (of the kind in Fig. 7) would not have been meaningful. This was a major reason for building DSV1.

The absence of DS in Complex cells in the DSV1 model (Figs. 6*A*, 7*B*), which is in good agreement with experimental data (Figs. 1*C*, 6*A*), merits comment. As in previous models (Chariker et al., 2016, 2020), the Complex cells in DSV1 typically receive little feedforward input (from one to two LGN cells rather than four to five for Simple cells), a fact consistent with data (Alonso et al., 2001; Hirsch et al., 2003). Since DS in LGN input initiates DS in DSV1 cortical cells, it makes sense that Complex cells without that input should not be direction-selective. Complex cells in DSV1 get almost all of their excitatory drive from other E-cells in L4 through recurrent excitation, as in earlier models (Chance et al., 1999; Chariker et al., 2016).

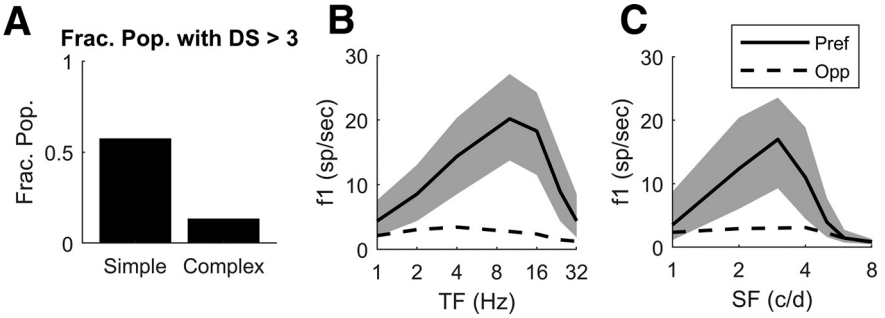

Figure 6. Model data on DS and firing rate as a function of TF and SF. ***A***, Fraction of model Simple and Complex cells with Pref/Opp > 3 (compare to Fig. 1*C*, experimental data); the fraction is computed on the population of $N = 2031$ Simple cells and 914 Complex cells in the central HC of the DSV1 model (Fig. 2*A*). ***B***, Pref and Opp firing rates as a function of TF for those model Simple cells with Pref/Opp > 3; $N = 1164$. Thick solid curve shows median Pref firing rate, with quartiles shown by the shaded areas. Dashed curve shows median Opp firing rates. ***C***, Pref and Opp firing rates as a function of SF for the same population of 1164 model Simple cells as in ***B*** with Pref/Opp > 3.

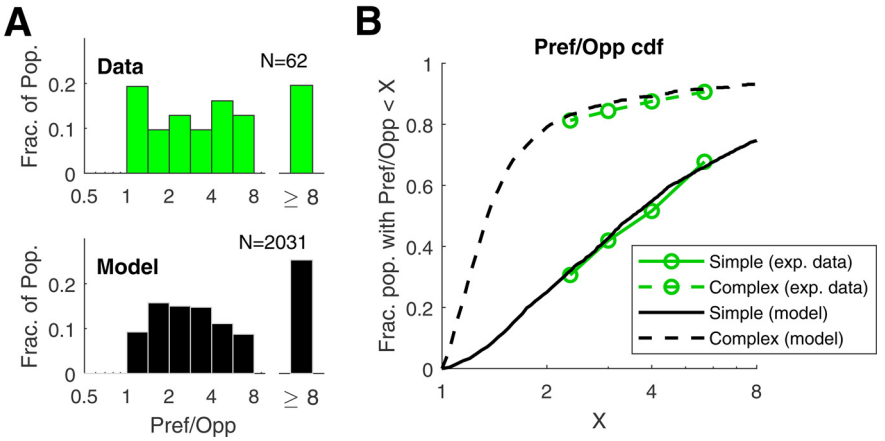

Figure 7. Population statistics of DS in model V1 neurons and comparison with V1 data. ***A***, Distribution of DS in model and data for Simple cells. The plots show the distributions of Pref/Opp in model and data for Simple cells for the <Ori, SF, TF> combination that produced maximum f1 response. The data histogram is plotted in green; the model histogram is plotted in black. ***B***, Cumulative distribution functions (CDFs) of Pref/Opp shown for Simple and Complex populations for data (green) and model (black).

We finish this section with the following two remarks: the first has to do with our use of f1 (as opposed to f0) in measurements of Pref and Opp for Simple cells, which we have done throughout this paper. We have found it natural to use f1 in layer 4Cα, the input layer to V1, to compare V1 Simple cells with their feedforward input. The feedforward input from LGN has DS only in f1: since individual LGN responses are not direction-specific, summed LGN spikes/s (= f0) are the same in both directions. However, it is different in cortical cell responses; both f0 and f1 responses of V1 Simple cells are direction-selective. In Simple cells in layer 4Cα, the Pref/Opp ratios computed using f1 and f0 are very similar, both in data and in DSV1. In both data and model, median Pref/Opp is ~3.0 for f0, while it is ~3.5 for f1. That cortical cells also have DS when measured in f0 could be significant functionally, as firing rates may play a role in communication between cortical layers or regions.

Our second remark is on methodology. DSV1 not only has DS cells but it emulates quantitatively the population distribution of DS derived from experiments (Figs. 6, 7). No other model has achieved this kind of agreement with cortical data on DS at the population level. We want to emphasize that the agreement between model and data were not achieved through curve-fitting. DSV1 is a mechanistic model; its network architecture is constrained by known micro-anatomy of V1, its neuronal interactions are designed to simulate those in real cortex, and like its predecessors (Chariker et al., 2016, 2018, 2020), its parameters are chosen so that the model, with a single set of parameters, replicates simultaneously many V1 phenomena including orientation selectivity, SF and TF tuning, contrast response, and γ-band oscillations.

Cortical contribution to DS in the DSV1 model

The mechanisms proposed by Chariker et al. (2021) guarantee that feedforward LGN inputs will have DS, but DS in a V1 cell's LGN input does not necessarily imply DS in the cell's response. LGN provides only a small fraction of the mean synaptic current into cortical cells; the bulk of it comes from intracortical synaptic transmission (Fig. 4; cf. Douglas and Martin, 2004), and intracortical activity could, in principle, modify DS in a cell's feedforward input. If intracortical currents modify a V1 cell's feedforward-DS, do they enhance or diminish it, and what are the mechanisms? Below, we answer these questions for the model. Given the quantitative agreement between DSV1 outputs and data, the findings are testable predictions for the real cortex.

Comparison of feedforward and cortical DS

The results are summarized in Figure 8.

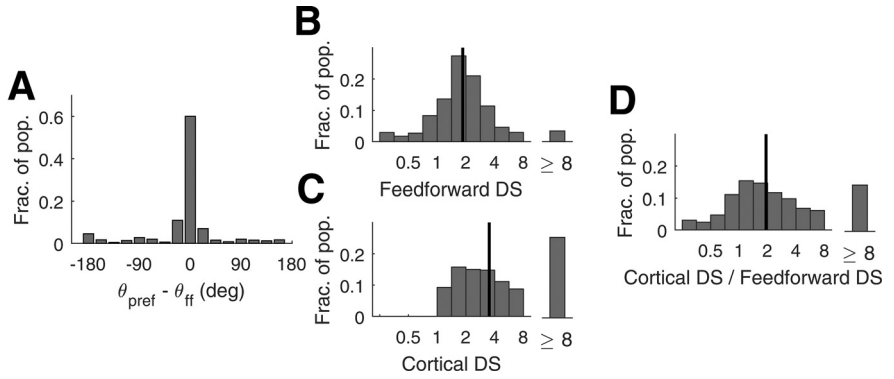

Figure 8. Comparison of DS in feedforward input current and in V1 firing rate for model Simple cells. ***A***, Deviations of cortical directional preference from those in feedforward LGN inputs. The statistics shown are for high DS (Pref/Opp > 3) Simple cells with two ON/OFF subregions in their receptive fields ($N = 659$). All cells were high DS cells in the central HC of the DSV1 model. The *x*-axis measures deviation of the cell's preferred direction from that of its LGN feedforward inputs. ***B***, Distribution of DS in the f1 response of the feedforward input current (FF-DS) to Simple cells. ***C***, Distribution of DS in the f1 response in V1 firing rate in Simple cells. ***D***, The distribution of the ratio of Cortex-DS/FF-DS cell-by-cell. In ***B–D***, the grating that optimizes f1 of the output spike train of the V1 cell is used as Pref in both FF-DS and Cortex-DS. Data are for all Simple cells in the central HC. Black vertical lines are medians; $N = 2031$.

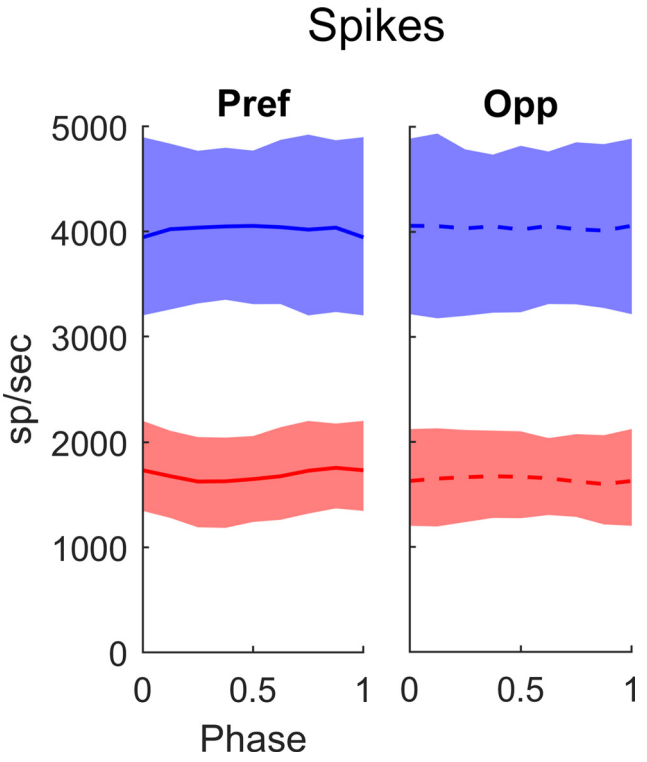

Figure 9. Summed spike rates received by L4 E cells from other L4 cells, in Pref and in Opp directions, plotted against LGN phase (as fractions of a cycle). The E-spikes received are plotted in red, I-spikes in blue. Medians are plotted as the solid (Pref) and dashed (Opp) curves; 25–75% quartiles are indicated by the shading. Data are from high DS cells in the central HC of DSV1; $N = 1164$. The stimuli were drifting gratings with SF = 3 c/d and TF = 10 Hz, near the peaks of the population tuning curves (like Fig. 6*B*,*C*). Here and in Figure 10, LGN phase is depicted as fraction of the stimulus cycle and is in the range [0,1] with 0 corresponding to peak spiking in the LGN input.

Preferred directions. The theory by Chariker et al. (2021) suggests that for a Simple V1 cell with two receptive field subregions, the preferred direction of its feedforward LGN inputs is from the OFF side to the ON side of the cell's receptive field. An immediate question is: Is this directional preference passed to the recipient cortical cell? The answer is Yes, as shown in Figure 8A. A majority (>3/4) of the high DS V1 cells with two subregions followed closely the preferred direction of their feedforward inputs, and fewer than 10% preferred the opposite (Fig. 8*A*).

Magnitudes of DS. DS in the output of a V1 cell, referred to here as Cortical-DS, is, as before, defined using as Pref the direction dictated by the stimulus that elicits maximum f1 response in the cell's firing rate. We will use the same stimulus to define DS in feedforward LGN inputs (abbreviated as FF-DS). Explicitly, FF-DS is computed by dividing f1 of the current resulting from the summed spiking LGN input in the Pref direction by f1 of the current from the spiking LGN input in the Opp direction, where the Pref and Opp directions are the same as in the computation of Cortical-DS.

The cortex enhances DS above what is present in the feedforward input: the median of Cortical-DS is nearly twice that of FF-DS (Fig. 8*B*,*C*). This can be seen in the population distributions of FF-DS and Cortical-DS (Fig. 8*B*,*C*). Data points are taken from all the Simple cells in the central HC of the DSV1 model. In Figure 8*C*, Cortical-DS is ≥ 1 by definition, but not so in Figure 8*B*. FF-DS is < 1 if LGN currents are modulated more in the direction opposite to the preferred direction of the postsynaptic V1 cell; this occurs for a small fraction of the cells, as reported in Figure 8*A*.

To give a sense of how FF-DS and Cortical-DS compare on a cell-by-cell basis in the model, Figure 8*D* plots a histogram of the ratio Cortical-DS/FF-DS. The histogram shows that while the median of Cortical-DS/FF-DS is around 2, the ratio has a wide spread from well below 1 to >8. In other words, while on average the cortical network doubles the Pref/Opp ratio, there is considerable diversity in the relations between the DS of cortical neurons and of their feedforward inputs.

Dynamic interaction of LGN and cortical currents

We present below a general theory of current interaction leading to a formula for cortical-DS that can help us understand how cortical interactions affect DS.

Synaptic conductances in Pref versus in Opp

In DSV1, there is no directional preference in the synaptic input from other cortical cells. This can be seen by examining the spike input to a model Simple cell from all its E-inputs and I-inputs from other cortical cells in L4 (Fig. 9). The summed rates shown in Figure 9 are drawn from the population of High DS Simple cells in the central HC of the DSV1 model. Observe that both summed E-spike rate (red) and summed I-spike rate (blue) have large DC levels that are approximately the same for Pref and Opp responses, and the same is true for summed spike rates from L6 (data not shown). In other words, synaptic input from other cortical cells is not direction-selective. In particular, the summed inhibitory synaptic conductance of high DS cells in DSV1 is not higher in Opp as proposed in some models (Suarez et al., 1995; Maex and Orban 1996; Freeman, 2021). For a

majority of the cells, there is also no significant dependence of synaptic conductance on LGN phase.

Phase relations between LGN and cortical currents

While synaptic conductance is flat with phase, the synaptic currents are modulated. The reason is that membrane potential modulation causes modulation of the driving forces of the synaptic currents. For a Simple cell, the membrane potential is modulated at the stimulus frequency f1; during the phase when LGN input is received, membrane potential is more depolarized than during the other half of the stimulus cycle (Fig. 10*A*). In the notation of the LIF equation (see Materials and Methods), a more positive value of V at LGN peak phase decreases the driving force for excitation E, $(V - V_E)$, and increases the driving force for inhibition I, $(V - V_I)$, where V_E and V_I are E and I reversal potentials. Because the E- and I-conductances caused by cortical synaptic connections to a target cell are approximately constant with phase (Fig. 9), the membrane potential modulation causes a significant increase in the magnitude of the I-current into a Simple cell when the LGN input is at its peak, and a slightly lowered E-current.

Through membrane potential modulation, the net cortical synaptic currents for most cells have a tendency to be antiphase with respect to the LGN current, and this is true in Pref as in Opp. Figure 10*B* shows the results for a large population of Simple cells in DSV1. Each point in Figure 10*B* is for one cell in the model: f1 amplitude is plotted on the vertical axis and phase is on the horizontal. Phase is plotted as fraction of stimulus period from 0 to 1, 0 being the phase where LGN peaks. The clusters of points near 0.5 phase in both Pref and Opp in Figure 10*B* confirm the theoretical expectation that the net (E + I) cortical synaptic currents should be antiphase with LGN input.

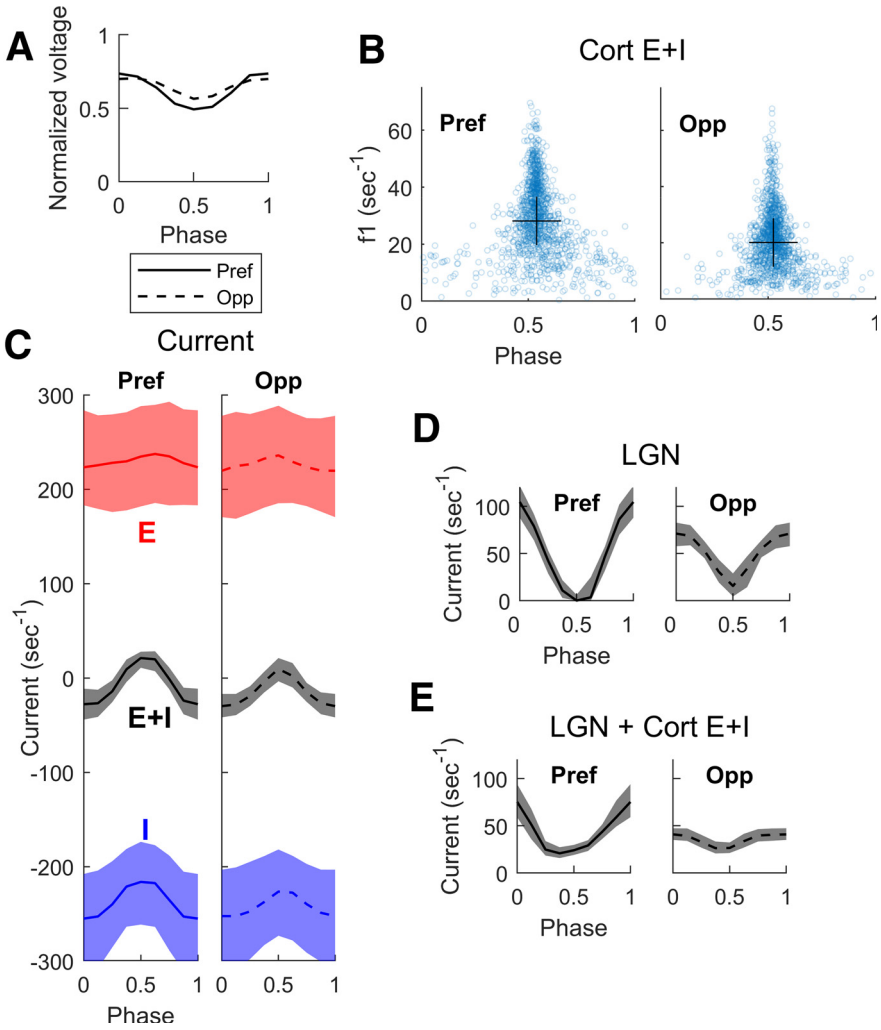

Figure 10. Membrane potential and cortical currents as function of LGN phase in the DSV1 model. Same cell population, stimuli and notation as in Figure 9. ***A***, Median modulation of membrane potential in Pref (solid) and Opp (dashed) directions. ***B***, The amplitude of the f1 component of net cortical synaptic current (E + I) plotted versus the phase (fraction of a cycle) of the E + I current with respect to the phase of LGN input. Data plotted for the Pref and Opp directions, for each cell in the population. In both directions, the cortical currents are predominantly out of phase (phase ~ 1/2 cycle) with LGN input. Crosses show medians for both *x*- and *y*-axes. ***C***, E and I synaptic currents versus phase with respect to LGN, in both Pref and Opp directions. E plotted in red, I in blue; medians and quartiles plotted for each. Gray curves and shaded regions are medians and quartiles of the net cortical current, E + I. ***D***, LGN excitatory current versus phase with respect to its peak, for Pref and Opp directions. Medians and quartiles plotted as in ***C***. ***E***, Sum of LGN and cortical currents, plotted versus phase with respect to LGN.

A formula for cortical-DS. Let {LGN}, {cortex}, and {LGN+cortex} denote, respectively, the f1 of LGN, net cortical, and LGN + cortical synaptic currents into a model cell. Then, if net cortical current is antiphase to LGN, we have

$$\{\text{LGN+cortex}\} \approx |\{\text{LGN}\} - \{\text{cortex}\}|.$$

To understand how cortex changes FF-DS, one must examine how the situation differs in the preferred and opposite directions. That is, one must compare

$$\text{cortical-DS} \approx \frac{|\text{Pref}\{\text{LGN}\} - \text{Pref}\{\text{cortex}\}|}{|\text{Opp}\{\text{LGN}\} - \text{Opp}\{\text{cortex}\}|} \qquad \text{R1}$$

to

$$\text{FF-DS} \approx \frac{|\text{Pref}\{\text{LGN}\}|}{|\text{Opp}\{\text{LGN}\}|}.$$

Whether or not Cortical-DS is larger or smaller than FF-DS depends on the relations among the four quantities in Equation R1, which we examine next, in Figure 10*C*–*E*.

Consider cortical E- and I-currents graphed in Figure 10*C*. The black curves with gray shading are the net cortical currents (= E + I), which are anti-phase with LGN, consistent with Figure 10*B*. Notice also in Figure 10*C* that while E- and I-currents each have a large variance, the variance of net cortical current (E + I) is much smaller as a consequence of the very tight balance between cortical E- and I-currents for each cell as illustrated earlier (Fig. 4). In Figure 10*D*, the excitatory summed LGN currents are graphed versus phase in the cycle, for both Pref and Opp directions, and we can see that they peak at 0 phase (the opposite

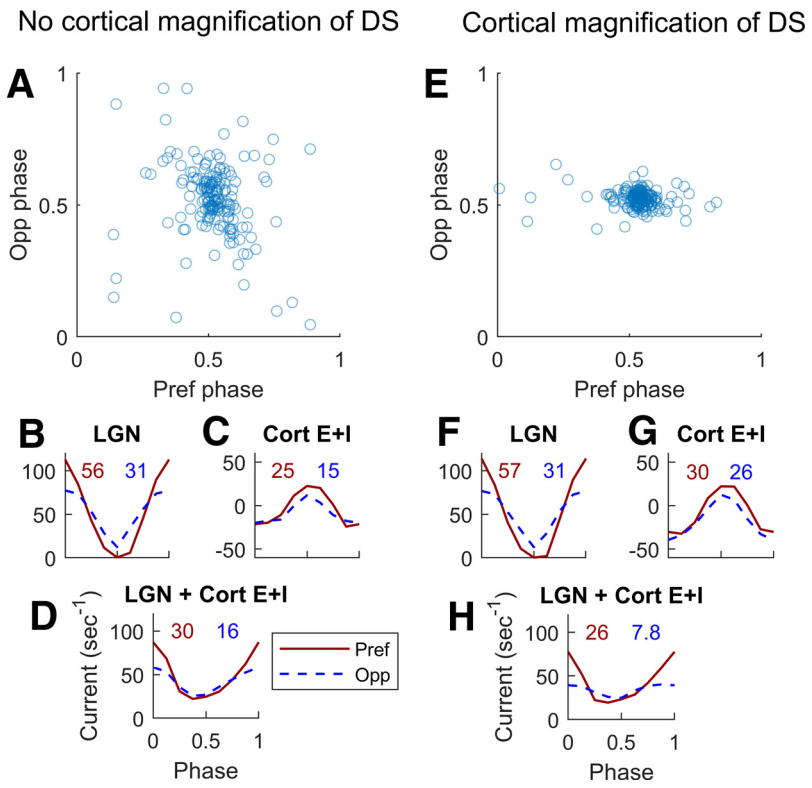

Figure 11. Dynamic interactions between cortical and feedforward synaptic currents in two groups of model L4 Simple DS cells. ***A–D***, From a group of 167 L4 cells that inherit all their DS and do not enhance it. ***E–H***, From a different group of 176 L4 cells, cells that enhance DS well above that in the LGN input. Both groups were selected to receive the same Pref/Opp ratio of ~1.8 in their LGN inputs. ***A***, Phase of membrane current versus LGN phase in response to a drifting grating <SF = 3 c/d, TF = 10 Hz>. Opp phase is plotted vertically, and Pref phase horizontally. Note the wide spread of the phases especially in Opp (SD = 0.14 in the Opp direction). ***B***, Medians of the cycle averages of LGN synaptic current; Pref (solid), Opp (dashed). F1 (in normalized units of s^{-1}) for the median are written above the plotted curves. ***C***, Corresponding median synaptic currents (E + I) for L4 cells in Pref and Opp directions. ***D***, Medians of the sums of LGN and cortical synaptic currents in Pref and Opp directions. The Pref/Opp ratio = 1.9 is roughly the same as for the LGN input in ***B***. ***E–H*** are analogous to ***A–D*** for the second group of cells. Note that in ***E***, the SD of the phase in the Opp direction (= 0.03) is much less than in ***A***, and the Pref/Opp ratio (= 3.3) of the Summed LGN + Cort E + I current is higher in ***H*** than in ***D***.

of the net cortical currents in Fig. 10*C*). The sum of LGN and cortical currents is graphed in Figure 10*E*. One can see in Figure 10*E* that the effect of cortical currents is to reduce the synaptic excitation from LGN, for both Pref and Opp directions. In DSV1, cortex reduces Opp current relatively more, and this causes cortical-DS > FF-DS for the population of High DS Simple cells (Fig. 10*E* vs *D*).

A detailed study of two subpopulations

To learn more about how the model enhances cortical DS, we study two subpopulations of L4 Simple cells: (1) a subpopulation that has DS similar to that of its feedforward input from LGN, and (2) a subpopulation that has cortical DS that is magnified compared with its feedforward input. Both populations consist of ~170 Simple cells, and both have 1.4 < FF-DS < 2. Interaction with cortex produces different results, however: cortical-DS < 2.5 for population 1, and cortical-DS > 4 for population 2.

We investigated how the model could generate such different outcomes in these two subpopulations, and observed the following difference in their phase distributions. Figure 11*A*,*E* are scatterplots of phase of net cortical currents in Pref versus Opp directions, using the same meaning of phase as in Figure 10*B*. The cells in population 2 almost all have cortical currents with a peak at 0.5 phase (Fig. 11*E*) but many cells in population 1 have current peaks significantly different from 0.5, especially in Opp (Fig. 11*A*).

The underlying difference in these two populations with regard to cortical magnification of DS lies in our previous analysis of the dynamics of cortical interactions. Figure 10*A* shows that modulations of the membrane potential *V* of a Simple cell follow the cell's feedforward LGN inputs, and that *V* has a minimum at midphase (i.e., at 0.5 cycle) with respect to LGN. When incoming spikes from cortex have little or no phase preference, cortical current peaks at ~0.5 phase as a consequence of the minimum of *V*. A cortical current peak at ~0.5 phase is the case for a majority of High DS cells in DSV1 (Fig. 10*B*), and also for almost all cells in population 2 (Fig. 11*E*). But when recurrent spike rates vary with phase, their synaptic inputs could interfere with the feedforward modulation of *V* and, in this way, could compromise the f1 of cortical current as well as cause its preferred phase to be displaced.

The difference in recurrent dynamics appears to be what is happening in the two populations in the Opp direction: phases in population 1 are more diffused than in population 2 (Fig. 11*A*,*E*), and the f1 of cortical E + I in population 1 is also smaller than that in population 2 (Fig. 11*C*,*G*). Differences of f1 in Pref are less significant. Thus, in population 2, interaction with cortex leads to the subtraction of a larger number from the denominator in Equation R1 compared with population 2. Subtraction of a larger number from the denominator causes the resulting Pref/Opp ratio to be larger, hence cortex magnifies DS more in population 2.

Discussion

The DSV1 model: aims and predictions

Aims of study and summary of findings

First, we found that the ON/OFF hypothesis that was analyzed in an idealized two-neuron scenario (Chariker et al., 2021) could work also in a biologically-realistic, large-scale network model, DSV1. The sparseness of LGN posed significant challenges in LGN template design but the templates did produce feedforward DS (Fig. 8*B*). Second, our results dispelled the concern mentioned in the Introduction that feedforward input would be too small to initiate DS in the firing rates of V1 neurons. In DSV1, E- and I-currents are so tightly balanced that LGN inputs, which break the balance, have a large effect (Fig. 4), and dynamic interaction of feedforward and intracortical currents leads to DS enhancement (Figs. 8-11). Comparisons of DSV1 output with experimental data (Figs. 5-7) show that the ON/OFF dynamic differences together with non-DS recurrent cortical interactions, without intracortical connections designed specifically to promote DS, effectively simulate the amount and quality of DS seen in V1 data.

The concept that DS in DSV1 is initiated by feedforward input is somewhat reminiscent of earlier work on orientation selectivity by Ferster et al. (1996). Our results add the major insight that cortex does not amplify a weak feedforward signal but instead is highly sensitive to feedforward input because of E-I balance (van Vreeswijk and Sompolinsky, 1996), and it enhances selectivity by suppressing, roughly equally, both nonpreferred and preferred responses (Fig. 10). The DSV1 model may provide mechanisms for cortical nonlinearity that has been observed by Priebe and Ferster (2005) to sharpen DS, but this is beyond the scope of the present paper.

We do not claim that the mechanisms proposed in this paper are the only mechanisms for DS, only that they are sufficient for producing the DS seen in data.

Model predictions

One of the purposes of a theory is to stimulate experiments to confirm or refute its predictions. Below are some important specific predictions. Given the variability in the real cortex, we predict that the following would hold for most (but not all) cells.

1. The preferred direction of a DS layer L4 Simple cell with two ON-OFF subfields should be motion from the OFF side to the ON side of the receptive field (Fig. 8*A*).
2. The physical distance d between rows of ON and OFF LGN cells in the LGN input to a V1 cell determines the range of SF to which a cortical cell responds with a consistent directional preference (Figs. 5, 6).
3. On average across the cortical population, the DS of a L4 cell is much greater than the DS in its feedforward input but there is a wide diversity in the degree of enhancement of DS in the cortex (Figs. 8, 10).
4. Net cortical inhibition, in antiphase with feedforward excitation from LGN, enhances cortical DS (Figs. 10, 11).

Context: other models

The significance of the DSV1 model can be understood in the context of many earlier models of DS. The earlier models fall into two main groups: (1) feedforward models and (2) intracortical models.

Feedforward models of DS

Many investigators have proposed, as we do, that STI in the feedforward input to the cortex initiates cortical DS (McLean and Palmer, 1989; Priebe and Ferster, 2005; Saul et al., 2005; Lien and Scanziani, 2018; Billeh et al., 2020). But what are the neural mechanisms responsible for STI? Our proposed answer is the small dynamic difference between the visual responses of ON and OFF LGN cells (Chariker et al., 2021) together with the well-known segregation of ON and OFF cells into distinct subregions (Hubel and Wiesel, 1962; Reid and Alonso, 1995). Below, we contrast our proposal with previous work.

One early proposal was that there are different types of LGN cells, so-called lagged and nonlagged cells, with very different temporal kernels (Saul and Humphrey, 1992a). The lagged-cell mechanism has been invoked to explain DS data in cat (Saul and Humphrey, 1992b) and ferret (Moore et al., 2005) V1. While the motion-energy model (Adelson and Bergen, 1985) was not concerned with biological implementation, later work on biological mechanisms of the motion-energy model proposed that the lagged-cells could be the source of STI (Emerson et al., 1992). However, lagged cells have not been found in macaque LGN (Wiesel and Hubel, 1966; Kaplan and Shapley, 1982; Hicks et al., 1983; Derrington and Lennie, 1984) and therefore the source of DS in macaque V1 must come from other mechanisms (Saul et al., 2005). Furthermore, the lagged cell mechanism would have trouble explaining the broad-band nature of DS in macaque especially the high value of the Pref/Opp ratio at high TF (Fig. 1*D*).

A number of studies have suggested that STI leading to DS comes from the differential timing of Transient and Sustained input to DS cortical cells (Marr and Ullman, 1981). Some experimentalists suggest (McLean and Palmer, 1989; Priebe and Ferster, 2005), and some theories propose, Sustained and Transient LGN→cortex connections (Lien and Scanziani, 2018; Billeh et al., 2020) as the source of cortical DS. One problem for Sustained-Transient models in macaque is that there is no evidence for a Sustained type of a Magnocellular input to macaque V1 layer 4Cα (Derrington and Lennie, 1984; Reid and Shapley, 2002; Saul et al., 2005). A second problem that has not been answered by Sustained-Transient models: how can a cortical cell select Sustained LGN input for one receptive field subregion and Transient LGN input for a spatially-distinct subregion? This is the wiring problem that is solved in DSV1 by the OFF-ON hypothesis together with the known ON-OFF segregation into subregions.

Intracortical models

Others proposed that the feedforward input to the cortex is not DS but rather that there was, initially, the generation of non-DS Transient and Sustained cortical RFs in cortical cells (De Valois et al., 2000; Baker and Bair, 2012). When these cortical cells' activity was combined intracortically, it would give rise to DS (De Valois et al., 2000; Baker and Bair, 2012). There are two distinct problems with the specific models proposed. De Valois et al. (2000) proposed that the Sustained branch of their model was comprised of cortical Simple cells that received Parvocellular feedforward input, while the Transient branch was cortical cells excited by Magnocellular LGN cells. This is not plausible for cells in layer 4Cα that receive predominantly Magnocellular LGN input (Lund, 1988; Chatterjee and Callaway, 2003; Angelucci and Sainsbury, 2006). Furthermore, DS is present at low contrast (Saul et al., 2005), and only M-cells provide useable responses at low contrast (Kaplan and Shapley, 1982; Hicks et al., 1983; Derrington and Lennie, 1984). The model of Baker and Bair (2012) resembles that of De Valois et al. (2000) without being species-specific. Neither model answers the question specific to layer 4Cα, namely, how is DS produced in such abundance (Figs. 1*C*, 7) at such an early stage in cortical signal processing?

Another very different kind of intracortical model of DS is that the excitatory drive of a DS cell is not DS but rather that inhibitory corticocortical input selectively suppresses responses in the nonpreferred direction (Suarez et al., 1995; Maex and Orban 1996; Freeman, 2021). This kind of theory is not consistent with experimental data that indicate that intracortical inhibitory conductance is somewhat higher amplitude in the Pref direction (Priebe and Ferster, 2005).

Modeling approach compared with machine learning (ML)

It is instructive to compare our modeling approach to ML, an increasingly important investigative tool in neuroscience. ML involves training large neural networks such as Convolutional Neural Networks, or CNNs, to perform specific tasks (Bashivan et al., 2019; Zhang et al., 2019). The strength of ML lies in the fact that it can deal with high-dimensional complexity and requires no a priori knowledge of anatomy or of how the brain performs the tasks. The price one pays for this "black-box" type approach that focuses on input-output relations is that they are

not designed to inform about mechanisms, and extracting such information can be extremely challenging. We have, in this paper, employed a bottom-up approach. In DSV1, which employs 36,000 model neurons, there is a direct correspondence between anatomic and model structures. Model components and functions were benchmarked to provide a comparison with their counterparts in real cortex. Consequently, one can expect that the dynamics of the DSV1 model are a good reflection of the underlying processes in real cortex; they have the potential to explain the neuronal circuit mechanisms.

The usefulness of a biologically realistic model goes beyond the model itself: it provides a well-constrained feedforward component to the next stages of processing in cortex. As layer 4Cα provides the dominant input to layer 4B in V1, DSV1 will provide an essential contribution to the modeling of layer 4B, and potentially even to the modeling of extrastriate cortical areas that receive input from layer 4B such as the thick stripes of V2 (Sincich and Horton, 2005; Federer et al., 2009) and MT (Sincich and Horton, 2005).

References

Adelman JP, Maylie J, Sah P (2012) Small-conductance Ca2+-activated K+ channels: form and function. Annu Rev Physiol 74:245–269.

Adelson EH, Bergen JR (1985) Spatiotemporal energy models for the perception of motion. J Opt Soc Am A 2:284–299.

Alonso JM, Usrey WM, Reid RC (2001) Rules of connectivity between geniculate cells and simple cells in cat primary visual cortex. J Neurosci 21:4002–4015.

Angelucci A, Sainsbury K (2006) Contribution of feedforward thalamic afferents and corticogeniculate feedback to the spatial summation area of macaque V1 and LGN. J Comp Neurol 498:330–351.

Baker PM, Bair W (2012) Inter-neuronal correlation distinguishes mechanisms of direction selectivity in cortical circuit models. J Neurosci 32:8800–8816.

Barkai E (2005) Dynamics of learning-induced cellular modifications in the cortex. Biol Cybern 92:360–366.

Bashivan P, Kar K, DiCarlo JJ (2019) Neural population control via deep image synthesis. Science 364:eaav9436.

Beaulieu C, Kisvarday Z, Somogyi P, Cynader M, Cowey A (1992) Quantitative distribution of GABA-immunopositive and -immunonegative neurons and synapses in the monkey striate cortex (area 17). Cereb Cortex 2:295–309.

Billeh YN, Cai B, Gratiy SL, Dai K, Iyer R, Gouwens NW, Abbasi-Asl R, Jia X, Siegle JH, Olsen SR, Koch C, Mihalas S, Arkhipov A (2020) Systematic integration of structural and functional data into multi-scale models of mouse primary visual cortex. Neuron 106:388–403.

Callaway E (1998) Local circuits in primary visual cortex of the macaque monkey. Annu Rev Neurosci 21:47–74.

Chance FS, Nelson SB, Abbott LF (1999) Complex cells as cortically amplified simple cells. Nat Neurosci 2:277–282.

Chariker L, Shapley R, Young LS (2016) Orientation selectivity from very sparse LGN inputs in a comprehensive model of macaque V1 cortex. J Neurosci 36:12368– 12384.

Chariker L, Shapley R, Young LS (2018) Rhythm and synchrony in a cortical network model. J Neurosci 38:8621–8634.

Chariker L, Shapley R, Young LS (2020) Contrast response in a comprehensive network model of macaque V1. J Vis 20:16.

Chariker L, Shapley R, Hawken MJ, Young LS (2021) A theory of direction selectivity for macaque primary visual cortex. Proc Natl Acad Sci U S A 118:e2105062118.

Chatterjee S, Callaway EM (2003) Parallel colour-opponent pathways to primary visual cortex. Nature 426:668–671.

Connolly M, Van Essen D (1984) The representation of the visual field in parvicellular and magnocellular layers of the lateral geniculate nucleus in the macaque monkey. J Comp Neurol 226:544–564.

DeFelipe J, González-Albo MC, Del Río MR, Elston GN (1999) Distribution and patterns of connectivity of interneurons containing calbindin, calretinin, and parvalbumin in visual areas of the occipital and temporal lobes of the macaque monkey. J Comp Neurol 412:515–526.

Denève S, Machens CK (2016) Efficient codes and balanced networks. Nat Neurosci 19:375– 382.

Derrington AM, Lennie P (1984) Spatial and temporal contrast sensitivities of neurones in lateral geniculate nucleus of macaque. J Physiol 357:219–240.

De Valois RL, Cottaris NP, Mahon LE, Elfar SD, Wilson JA (2000) Spatial and temporal receptive fields of geniculate and cortical cells and directional selectivity. Vision Res 40:3685–3702.

Douglas RJ, Martin KAC (2004) Neuronal circuits of the neocortex. Annu Rev Neurosci 27:419–451.

Emerson RC, Bergen JR, Adelson EH (1992) Directionally selective complex cells and the computation of motion energy in cat visual cortex. Vision Res 32:203–218.

Federer F, Ichida JM, Jeffs J, Schiessl I, McLoughlin N, Angelucci A (2009) Four projection streams from primate V1 to the cytochrome oxidase stripes of V2. J Neurosci 29:15455–15471.

Ferster D, Sooyoung C, Wheat H (1996) Orientation selectivity of thalamic input to simple cells of cat visual cortex. Nature 380:249–252.

Fitzpatrick D, Lund JS, Blasdel GG (1985) Intrinsic connections of macaque striate cortex: afferent and efferent connections of lamina 4C. J Neurosci 5:3329–3349.

Freeman AW (2021) A model for the origin of motion direction selectivity in visual cortex. J Neurosci 41:89– 102.

Garcia-Marin V, Kelly JG, Hawken MJ (2019) Major feedforward thalamic input into layer 4C of primary visual cortex in primate. Cereb Cortex 29:134– 149.

Hansel D, Sompolinsky H (1997) Modeling feature selectivity in local cortical circuits. In: Methods in neuronal modeling, from synapse to networks, Chapter 13 (Koch C, Segev I, eds). Cambridge: The MIT Press.

Hansel D, van Vreeswijk C (2012) The mechanism of orientation selectivity in primary visual cortex without a functional map. J Neurosci 32:4049–4064.

Hawken MJ, Parker AJ (1984) Contrast sensitivity and orientation selectivity in lamina IV of the striate cortex of Old World monkeys. Exp Brain Res 54:367–372.

Hawken MJ, Parker AJ, Lund JS (1988) Laminar organization and contrast sensitivity of direction-selective cells in the striate cortex of the old-world monkey. J Neurosci 8:3541–3548.

Hawken MJ, Shapley RM, Grosof DH (1996) Temporal frequency selectivity in monkey visual cortex. Vis Neurosci 13:477–492.

Henry CA, Joshi S, Xing D, Shapley RM, Hawken MJ (2013) Functional characterization of the extraclassical receptive field in macaque v1: contrast, orientation, and temporal dynamics. J Neurosci 33:6230–6242.

Hicks TP, Lee BB, Vidyasagar TR (1983) The responses of cells in macaque lateral geniculate nucleus to sinusoidal gratings. J Physiol 337:183–200.

Hirsch JA, Martinez LM, Pillai C, Alonso JM, Wang Q, Sommer FT (2003) Functionally distinct inhibitory neurons at the first stage of visual cortical processing. Nat Neurosci 6:1300– 1308.

Holmgren C, Harkany T, Svennenfors B, Zilberter Y (2003) Pyramidal cell communication within local networks in layer 2/3 of rat neocortex. J Physiol 551:139–153.

Hubel DH, Wiesel TN (1962) Receptive fields, binocular interaction and functional architecture in the cat's visual cortex. J Physiol 160:106–154.

Jin J, Wang Y, Lashgari R, Swadlow HA, Alonso JM (2011) Faster thalamocortical processing for dark than light visual targets. J Neurosci 31:17471–17479.

Kaplan E, Shapley R (1982) X and Y cells in the lateral geniculate nucleus of the macaque monkey. J Physiol 330:125–143.

Kaplan E, Purpura K, Shapley RM (1987) Contrast affects the transmission of visual information through the mammalian lateral geniculate nucleus. J Physiol 391:267–288.

Knight BW (1972) Dynamics of encoding in a population of neurons. J Gen Physiol 59:734–766.

Levitt JB, Schumer RA, Sherman SM, Spear PD, Movshon JA (2001) Visual response properties of neurons in the LGN of normally reared and visually deprived macaque monkeys. J Neurophysiol 85:2111–2129.

Lien AD, Scanziani M (2018) Cortical direction selectivity emerges at convergence of thalamic synapses. Nature 558:80–86.

Lin IC, Xing D, Shapley R (2012) Integrate-and-fire vs Poisson models of LGN input to V1 cortex: noisier inputs reduce orientation selectivity. J Comput Neurosci 33:559–572.

Lund JS (1988) Anatomical organization of macaque monkey striate visual cortex. Annu Rev Neurosci 11:253–288.
McLean J, Palmer LA (1989) Contribution of linear spatiotemporal receptive field structure to velocity selectivity of simple cells in area 17 of cat. Vision Res 29:675–679.
Maex R, Orban GA (1996) Model circuit of spiking neurons generating directional selectivity in simple cells. J Neurophysiol 75:1515–1545.
Marr D, Ullman S (1981) Directional selectivity and its use in early visual processing. Proc R Soc London Ser B 211:151–180.
Masland RH (2012) The neuronal organization of the retina. Neuron 76:266–280.
Moore BD, Alitto HJ, Usrey WM (2005) Orientation tuning, but not direction selectivity, is invariant to temporal frequency in primary visual cortex. J Neurophysiol 94:1136–1345.
Oswald AM, Reyes AD (2011) Development of inhibitory timescales in auditory cortex. Cereb Cortex 21:1351–1361.
Priebe NJ, Ferster D (2005) Direction selectivity of excitation and inhibition in simple cells of the cat primary visual cortex. Neuron 45:133–145.
Reichardt W (1961) Autocorrelation, a principle for the evaluation of sensory information by the central nervous system. In: Sensory communication (Rosenblith WA, ed). New York: Wiley.
Reid RC, Alonso JM (1995) Specificity of monosynaptic connections from thalamus to visual cortex. Nature 378:281–284.
Reid RC, Shapley RM (2002) Space and time maps of cone photoreceptor signals in macaque lateral geniculate nucleus. J Neurosci 22:6158–6175.
Ringach DL, Shapley RM, Hawken MJ (2002) Orientation selectivity in macaque V1: diversity and laminar dependence. J Neurosci 22:5639–5651.
Saul AB, Humphrey AL (1992a) Evidence of input from lagged cells in the lateral geniculate nucleus to simple cells in cortical area 17 of the cat. J Neurophysiol 68:1190–1208.
Saul AB, Humphrey AL (1992b) Temporal-frequency tuning of direction selectivity in cat visual cortex. Vis Neurosci 8:365–372.
Saul AB, Carras PL, Humphrey AL (2005) Temporal properties of inputs to direction-selective neurons in monkey V1. J Neurophysiol 94:282–294.
Silveira LC, Perry VH (1991) The topography of magnocellular projecting ganglion cells (M-ganglion cells) in the primate retina. Neurosci 40:217–237.
Sincich LC, Horton JC (2005) The circuitry of V1 and V2: integration of color, form, and motion. Annu Rev Neurosci 28:303–326.
Skottun BC, De Valois RL, Grosof DH, Movshon JA, Albrecht DG, Bonds AB (1991) Classifying simple and complex cells on the basis of response modulation. Vision Res 31:1079–1086.
Stratford KJ, Tarczy-Hornoch K, Martin KA, Bannister NJ, Jack JJ (1996) Excitatory synaptic inputs to spiny stellate cells in cat visual cortex. Nature 382:258–261.
Suarez H, Koch C, Douglas R (1995) Modeling direction selectivity of simple cells in striate visual cortex within the framework of the canonical microcircuit. J Neurosci 15:6700–6719.
Turrigiano G (2012) Homeostatic synaptic plasticity: local and global mechanisms for stabilizing neuronal function. Cold Spring Harb Perspect Biol 4:a005736.
van Vreeswijk C, Sompolinsky H (1996) Chaos in neuronal networks with balanced excitatory and inhibitory activity. Science 274:1724–1726.
Watson AB, Ahumada AJ (1983) A look at motion in the frequency domain. NASA Tech Mem 84352.
Watson AB, Ahumada AJ (1985) Model of human visual-motion sensing. J Opt Soc Am A 2:322–341.
Wiesel TN, Hubel DH (1966) Spatial and chromatic interactions in the lateral geniculate body of the rhesus monkey. J Neurophysiol 29:1115–1156.
Yoshioka T, Levitt JB, Lund JS (1994) Independence and merger of thalamocortical channels within macaque monkey primary visual cortex: anatomy of interlaminar projections. Vis Neurosci 11:467–489.
Zhang Y, Lee TS, Li M, Liu F, Tang S (2019) Convolutional neural network models of V1 responses to complex patterns. J Comput Neurosci 46:33–54.
Zhu W, Shelley M, Shapley R (2009) A neuronal network model of primary visual cortex explains spatial frequency selectivity. J Comput Neurosci 26:271–287.
Zilles K, Palomero-Gallagher N, Schleicher A (2004) Transmitter receptors and functional anatomy of the cerebral cortex. J Anat 205:417–432.